The Physics of Mesoscopic Systems

Dietmar Weinmann

E-mail: weinmann@ipcms.u-strasbg.fr

Institut de Physique et Chimie des Matériaux de Strasbourg
UMR 7504, CNRS-ULP
23, rue du Loess
67037 Strasbourg Cedex
France

March 30, 2005

Lectures held during the
Seventh Petra School of Physics
17–22 September 2000
at the University of Jordan

Abstract

An ongoing tendency in modern material science is to propose and to investigate systems containing smaller and smaller structures. The resulting systems approach the mesoscopic regime in which the quantum phase coherence leads to important corrections to the electronic properties of the devices. At the same time, microscopic details of the sample, like the exact impurity configuration in disordered systems, determine some quantitative features of the behavior. This can lead to pronounced fluctuations of a quantity measured in different samples which are macroscopically equivalent.

This aim of this series of lectures is to introduce the mesoscopic regime and to review a selection of the most important effects appearing in mesoscopic systems. The theory of electronic transport in mesoscopic samples is illustrated in the framework of the Landauer approach in which the conductance is determined by the scattering properties of the sample. As an example for the importance of electron-electron interactions for the conductance, we describe the Coulomb blockade effect appearing in devices containing ultra-small tunnel junctions or quantum dots. The importance of mesoscopic effects for basic research, as well as for applications in nanoelectronic devices and for metrology, is stressed.

Contents

1 Introduction to the Physics of Mesoscopic Systems 4
- 1.1 The Mesoscopic Regime 4
- 1.2 Prominent Mesoscopic Effects 6
  - 1.2.1 Aharonov-Bohm Oscillations 6
  - 1.2.2 The Integer Quantum Hall Effect 8
  - 1.2.3 The Fractional Quantum Hall Effect 11
  - 1.2.4 Universal Conductance Fluctuations 12
  - 1.2.5 Conductance Quantization in Quantum Point Contacts 13
  - 1.2.6 Persistent Currents in Mesoscopic Rings 14

2 Theory of Electronic Transport in Mesoscopic Structures 19
- 2.1 Breakdown of Classical Transport 19
- 2.2 Linear Response Theory 20
  - 2.2.1 Definition of the Conductance 23
- 2.3 The Landauer Approach 23
  - 2.3.1 One-Channel Two-Point Conductance 24
  - 2.3.2 Multi-Channel Two-Point Conductance 28
  - 2.3.3 Edge States and Quantum Hall Effect 29
- 2.4 Resonant *versus* Sequential Tunneling 33
  - 2.4.1 Resonant Tunneling 33
  - 2.4.2 Sequential Tunneling 35

3 Effects of the Electron-Electron Interaction 37
- 3.1 The Coulomb Blockade 37
- 3.2 Transport through Quantum Dots 40
- 3.3 The Single Electron Transistor 41
  - 3.3.1 Transport Spectroscopy 42
  - 3.3.2 Applications 44

4 Summary 44

References 46

1 Introduction to the Physics of Mesoscopic Systems

At the end of the XX$^{\text{th}}$ century, a clear tendency towards nanostructured systems appears in physical material science. This includes semiconductor structures and magnetic materials, but also intrinsically nanostructured systems like biomaterials and macromolecules. These smaller and smaller structures approach the so-called mesoscopic regime in which quantum effects become relevant for the behavior of the materials. At the same time, considerable advances in the controlled fabrication of submicron solid state structures, as well as the common availability of low temperature facilities, have allowed for a systematic investigation of artificially made structures whose electronic properties are modified or even dominated by quantum interference effects. This makes it possible to perform experiments in the mesoscopic regime which directly probe quantum properties of phase coherent many-body systems.

Good starting points to the studying of mesoscopic physics are recent books on the subject by Y. Imry [1], S. Datta [2], and the somewhat more advanced chapters in reference [3].

In the following, we present an elementary introduction to selected aspects of the physics of mesoscopic systems.

1.1 The Mesoscopic Regime

The mesoscopic regime is the intermediate one between the quantum world of microscopic systems (atoms or small molecules) and the classical world of macroscopic systems like large pieces of condensed matter. Mesoscopic systems typically consist of a large number of atoms, but their behavior is considerably influenced by quantum interference effects. This situates mesoscopic physics at the interface of statistical physics and quantum physics.

The quantum phase coherence, needed for the appearance of interference effects, is conserved only during a finite time τ_ϕ, called the phase breaking time. The phase coherence is lost when the system or its components under investigation interact with its environment, as for instance by an electron-phonon scattering event. In electronic conductors, the finite phase breaking time corresponds to a phase breaking length L_ϕ over which the electrons can travel before their phase coherence is lost.

Mesoscopic quantum effects appear when the typical time or length scales of the system are smaller than the phase breaking time or length, respectively. In many cases this means that the relevant system size

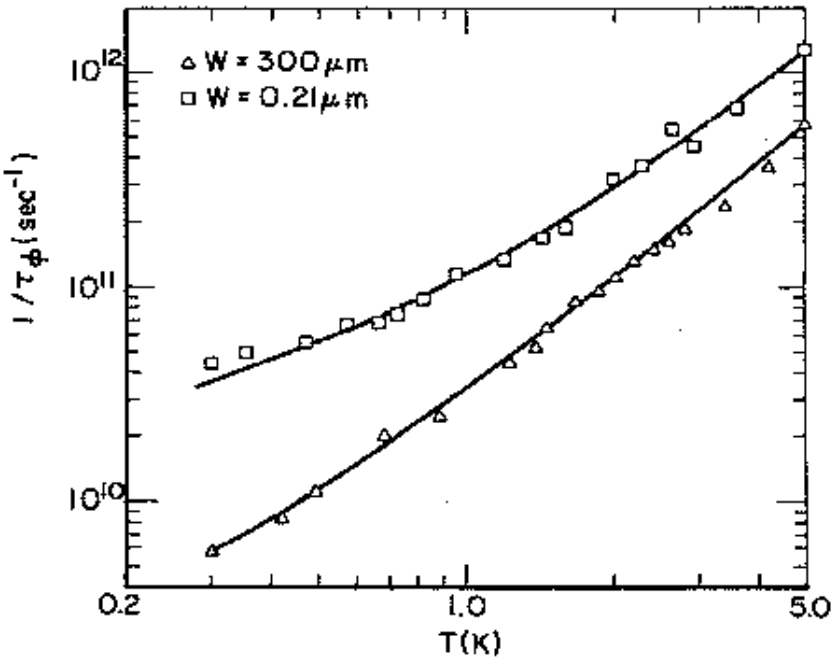

Figure 1: The temperature dependence of the phase coherence time in GaAs, measured in samples of different width W (from [4]).

L must be smaller than the phase coherence length

$$L < L_\phi \,. \tag{1}$$

For an electron, the phase coherence time/length is limited by electron-electron and electron-phonon scattering. These processes are important at high temperatures, but both types of scattering are suppressed at low temperatures such that the phase coherence time/length is strongly material and temperature dependent (see Figure 1).

It is important to note that only scattering processes during which an excitation (a phonon, electron-hole excitation, *etc.*) of the environment is created or destroyed, lead to a loss of phase coherence. Such scattering processes leave a trace of the particle in the environment which can in principle be observed and is reminiscent of a measurement of the trajectory of the particle. These processes are typically inelastic and connected to a transfer of energy. However, processes which alter the environment without energy transfer, e.g. by flipping a spin can also lead to decoherence.

In contrast, the scattering of the electrons off static impurities is always elastic. Even though the phase of the electrons may be modified

in the scattering process, this happens in a well-defined way and does not destroy the phase coherence effects. A more detailed discussion of this important distinction between elastic and inelastic scattering processes can be found in reference [1].

The mesoscopic regime is therefore characterized by small time and/or length scales and low temperatures. When the temperature is lowered, the phase coherence time/length increases and the mesoscopic regime is extended to larger time/length scales. At sub-Kelvin temperatures, the time and length scales in semiconductor samples are of the order of picoseconds and micrometers, respectively.

Since in mesoscopic physics one is often dealing with small finite systems at low temperatures, the electronic level spacing Δ of the discrete spectrum can become larger than the thermal energy $k_{\mathrm{B}}T$. Then, the precise details of the spectrum and not only global quantities like the mean density of states determine the electronic and thermodynamic properties of the sample. However, the precise spectrum depends on the impurity configuration leading to fluctuations of the observed quantities between macroscopically indistinguishable samples. These fluctuations themselves are an interesting quantity to study since the qualitative effects are often universal in the sense that they do not depend on on microscopic details.

1.2 Prominent Mesoscopic Effects

In this section, we briefly present a selection of the most important effects arising as a consequence of the quantum phase coherence of the electronic wave functions in the mesoscopic regime. Many of the most spectacular effects appear in samples of reduced dimension like two-dimensional electron gases in semiconductor heterostructures, one-dimensional systems (so-called quantum wires) and structures in which the electrons are completely confined, the so-called quantum dots. Most interesting for basic research and most promising in the view of applications are the electronic properties of such systems and we shall concentrate on them.

1.2.1 Aharonov-Bohm Oscillations

One of the most striking consequences of phase coherence is the possibility to observe Aharonov-Bohm oscillations in the conductance of mesoscopic structures containing small normal metal rings [5]. At low temperature, when the phase coherence length is larger than the circumference of the ring, the interference between the contributions of an electron going through one arm of the ring and the same electron going through the other arm of the ring is important. To the intrinsic

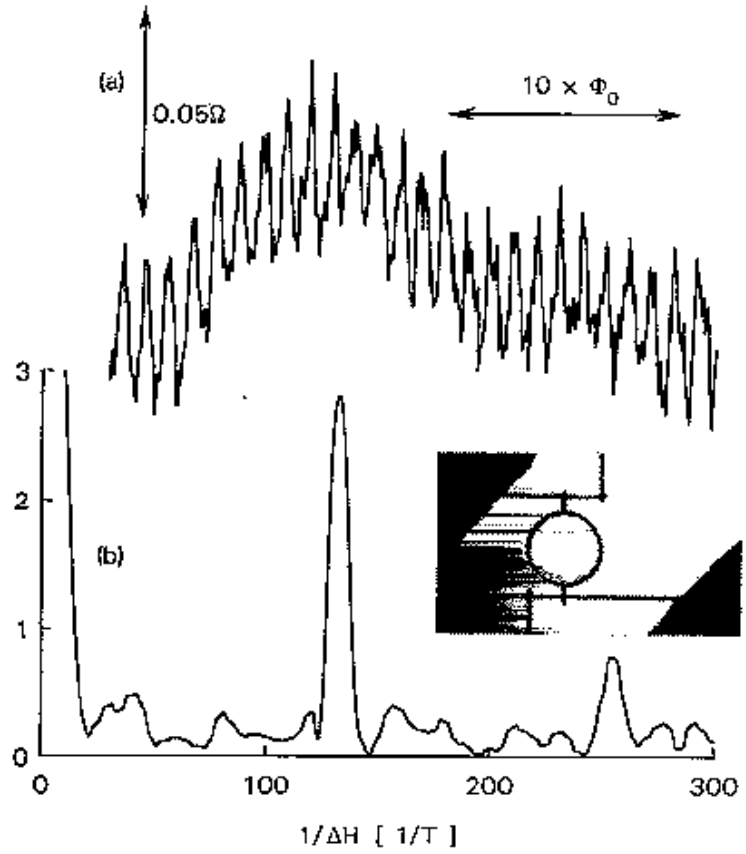

Figure 2: Observation of Aharonov-Bohm oscillations in the conductance of rings in a magnetic field. The figure shows (a) the conductance as a function of the magnetic field, (b) its Fourier transform showing the periodicity of the oscillations, and in the inset a picture of the sample (from [5]).

phase difference ϕ_0 of the two paths one has to add the effect of the magnetic field which leads to a phase shift given by

$$\phi_B = \frac{2\pi e}{h} \oint \mathrm{d}\vec{s}\vec{A} = \frac{2\pi e}{h}\Phi\,. \tag{2}$$

The integral over the vector potential $\vec{A}$ is to be performed on a closed path around the ring. This yields a phase shift proportional to the magnetic flux Φ through the ring, given by the area of the ring multiplied by the (constant) magnetic field strength B perpendicular to the plane of the ring. A component of the conductance (the ratio between the current through the sample and the applied voltage) is then proportional to $\cos(\phi_0 + \phi_B)$, leading to the observed h/e-periodic os-

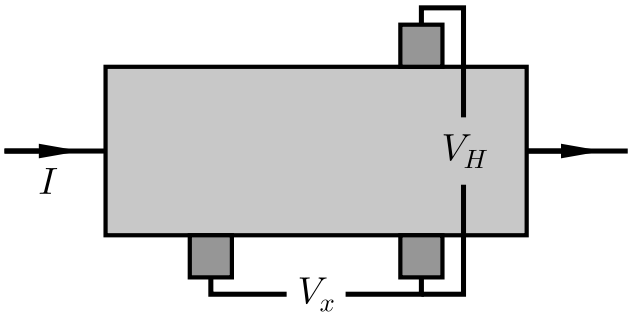

Figure 3: Hall-bar geometry. the longitudinal voltage V_x is measured between two points along the same edge of the sample while the Hall voltage $V_{\rm H}$ is measured between points at opposite sides of the samples. The magnetic field is applied perpendicular to the plane of the drawing.

cillations of the conductance of the device as a function of the magnetic flux piercing the ring as shown in figure 2.

1.2.2 The Integer Quantum Hall Effect

One of the first and most spectacular observations of macroscopic consequences of the phase coherence in the electronic properties of solid state devices was the discovery of the integer quantum Hall effect [6] by Klaus von Klitzing in 1980, rewarded with the Nobel prize in 1985. Von Klitzing used the two-dimensional electron gas formed in a silicon MOSFET device. To observe the Hall effect, one drives a current through the sample and measures the longitudinal voltage V_x and the transverse Hall voltage $V_{\rm H}$ (see figure 3), as a function of the strength of the magnetic field applied perpendicular to the plane of the two-dimensional electron gas.

The Hall effect predicts that when a conductor is placed in a magnetic field B, a transverse voltage between opposite lateral sides of the sample proportional to the longitudinal current I can be measured, given by

$$V_{\rm H} = R_{\rm H} I \,. \tag{3}$$

Classically, using the Drude formula, one gets the Hall resistance

$$R_{\rm H} = \frac{B}{e n_{\rm s}} \tag{4}$$

with the two-dimensional electron density $n_{\rm s}$. The longitudinal resistance R_x, calculated from the ratio of the voltage drop between two points on the same side of the sample to the current I, within

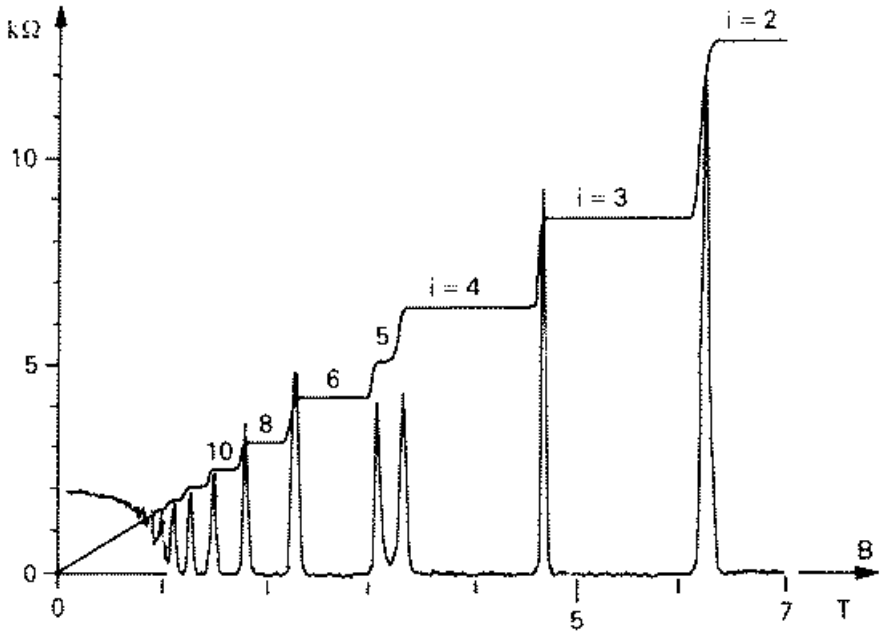

Figure 4: The magnetic field dependence of the longitudinal resistance (showing peaks at strong magnetic field) and the Hall resistance (being linear in the strength of the magnetic field according to the classical prediction and increasing in steps at strong magnetic field) in the integer quantum Hall effect regime. The values of the Hall resistance on the plateaus are $R_{\mathrm{H}} = h/ie^2$.

the Drude theory, is unaffected by the magnetic field. This behavior can be observed in the very left hand side of figure 4, in the regime of weak magnetic field. When the experiment is carried out at very low temperature in very strong magnetic field and using high mobility samples, the behavior is however completely different (see figure 4). The longitudinal resistance drops to zero except for a few values of the magnetic field where peaks appear. The Hall resistance exhibits steps at the positions where R_x is non-zero and plateaus of constant values in between. The values of R_{H} on these plateaus are given by h/ie^2 with integer numbers $i = \{1, 2, 3, \ldots\}$. It turns out that these values are reproducible with great precision and extremely robust against changing the chosen material, the size of the sample, or introducing a small concentration of impurities. This has important implications for the application of the quantum Hall effect in metrology where it is used since several years as a resistance standard.

In order to understand the origin of these features, one has to consider electrons in a two-dimensional system, subject to a strong

magnetic field. In a perfectly clean system, within a (semi-)classical picture, an electron moves on a so-called cyclotron orbit. These cyclotron orbits are circles of radius

$$r_{\mathrm{c}} = \frac{mv}{eB}\,, \tag{5}$$

where m is the effective mass and v the velocity of the electron. r_{c} shrinks inversely proportional to the strength of the magnetic field strength B. These cyclotron orbits become relevant for the behavior of the system when they are not destroyed by scattering processes. Thus, the condition

$$r_{\mathrm{c}} \ll l, L_{\phi} \tag{6}$$

with the mean free path l must be fulfilled. This is the case for pure materials at low temperatures in strong magnetic fields.

The mesoscopic effect due to the phase coherence appears in this case because the relevant length scale r_{c} for the behavior of the electrons becomes smaller than the phase coherence length even though the total extension of the sample may be much larger. In fact, typical quantum Hall effect measurements are done using samples of macroscopic dimensions, of the order of 1mm.

When the electrons move phase coherently on circular orbits, the energies of the electrons are quantized. A full quantum calculation [2] yields the so-called Landau levels, defining the allowed energies

$$E_n = \left(n + \frac{1}{2}\right)\hbar\omega_{\mathrm{c}}\,, \tag{7}$$

with the cyclotron frequency

$$\omega_{\mathrm{c}} = \frac{eB}{m}\,. \tag{8}$$

and the integer quantum number n. The energies of the Landau levels increase linearly with the strength of the magnetic field. They are highly degenerate and their degree of degeneracy per spin orientation is

$$N_{\mathrm{d}} = ABe/h\,, \tag{9}$$

where A is the area of the sample. N_{d} increases with the magnetic field strength B. The number of one-particle states per Landau level equals the number of flux quanta $\Phi_0 = h/e$ piercing the sample.

At low temperatures and high magnetic field, $k_{\mathrm{B}}T \ll \hbar\omega_{\mathrm{c}}$, and only the Landau levels below the Fermi energy are occupied. The filling factor ν gives the number of occupied Landau levels and is equivalent to the number of electrons per flux quantum inside the sample. When

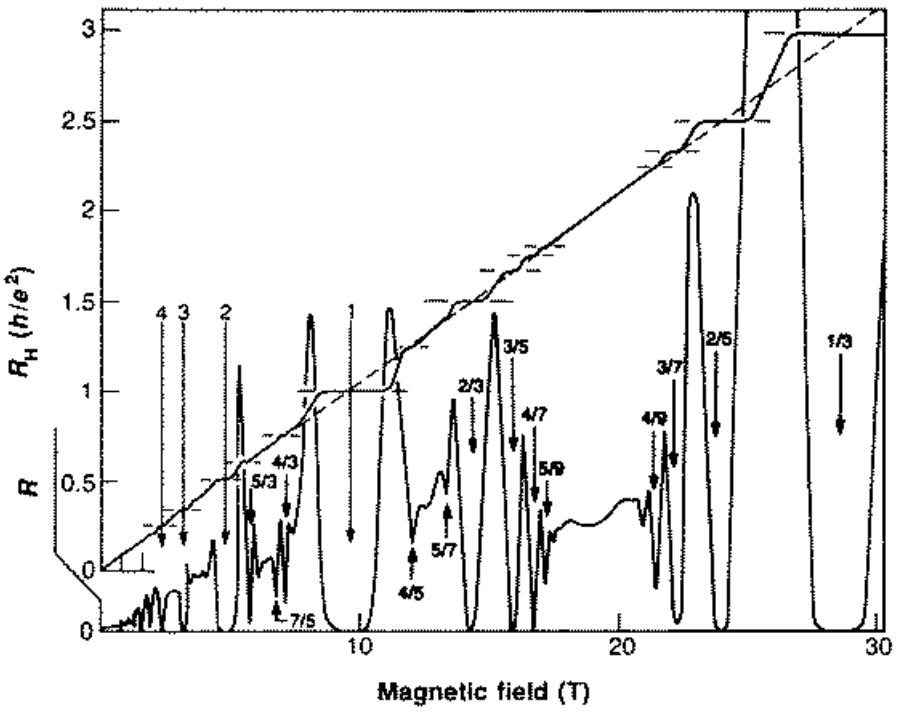

Figure 5: The Hall resistance and the longitudinal resistance in the fractional quantum Hall effect regime, showing additional plateaus and resistance minima, respectively, at fractional values of the filling factors.

the magnetic field is increased, one Landau level after the other crosses the Fermi energy and the filling factor decreases. The values of the magnetic field where the Landau levels are depopulated coincide with the positions of the peaks in the longitudinal resistance R_x and the steps in the Hall voltage $R_{\rm H}$. While the Fermi energy is between two Landau levels, the longitudinal resistance vanishes and $R_{\rm H}$ is constant. These features can be explained within the edge state picture which we shall present in section 2.3.3.

For a more advanced introduction to the integer quantum Hall effect, we refer the reader to the recent reference [1]. A detailed discussion of the earlier work on the integer and the fractional quantum Hall effect can be found in reference [7]. A recent overview can be found in reference [8].

1.2.3 The Fractional Quantum Hall Effect

Going to stronger magnetic fields and to lower temperatures in two-dimensional electron gases, one can observe additional plateaus of the

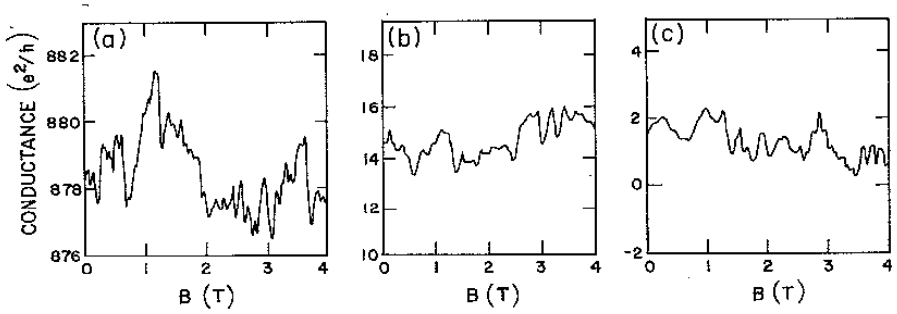

Figure 6: The reproducible fluctuations of the conductance as a function of the magnetic field for (a) a gold wire with a diameter of 0.8μm, (b) a narrow channel in the two-dimensional electron gas of a silicon MOSFET, and (c) a numerical simulation within the Anderson model. Even though the absolute values of the conductance are very different, the amplitude of the fluctuations is of the same order (from [12]).

Hall resistance at fractional filling factors like $\nu = 1/3$ (see figure 5). This so-called fractional quantum Hall effect has been discovered [9] in 1982. The features at fractional filling can be traced back to the existence of correlated collective quasi-particle excitations [10]. Thus, in contrast to the integer quantum Hall effect, the Coulomb interaction between the electrons is essential for the explanation of the fractional quantum Hall effect. The quasi-particles have fractional charge (for instance $e/3$ at $\nu = 1/3$). From shot noise measurements [11], it could be confirmed recently that the charge carriers at $\nu = 1/3$ in the fractional quantum Hall effect regime have indeed charge $e/3$. After this confirmation, Tsui, Störmer and Laughlin received the 1998 Nobel prize for the discovery and interpretation of the fractional quantum Hall effect. For a review of the early work on the fractional quantum Hall effect, see reference [7]. A more recent introduction can be found in reference [8].

1.2.4 Universal Conductance Fluctuations

The conductance of disordered wires in the mesoscopic regime exhibits pronounced fluctuations as a function of external parameters like the magnetic field or the Fermi energy (see figure 6). These fluctuations were discovered [13] in the low-temperature (below 1K) conductance of the inversion layer in a disordered silicon MOSFET. The fluctuations are perfectly reproducible and represent a fingerprint of the sample. The origin of the fluctuations lies in the interference of different ways the electrons can take when traveling through the sample, as sketched

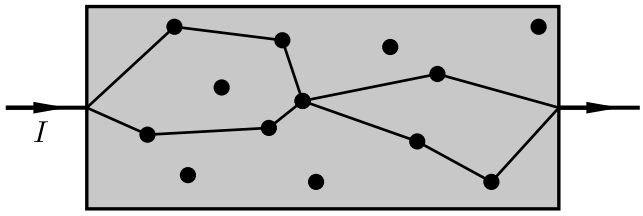

Figure 7: Possible paths of an electron through a disordered wire, with elastic scattering processes at impurities. The interference of such paths is influenced by a magnetic field or the value of the Fermi wave vector, leading to fluctuations of the conductance in the mesoscopic regime.

in figure 7.

In a macroscopically equivalent sample with a microscopically different impurity configuration, the fluctuations are qualitatively similar but their precise features can be completely different. The most striking feature of the conductance fluctuations is however the fact that their typical amplitude is universal in the diffusive regime [12]. Independently of the mean value of the conductance, the fluctuations are always of the order of the conductance quantum e^2/h and depend only on the basic symmetries (like time-inversion symmetry) of the system [14]. This can be traced to the repulsion of the eigenvalues of random transfer matrices. For further reading, we recommend reference [1] and chapter 1 of reference [3].

1.2.5 Conductance Quantization in Quantum Point Contacts

A point contact is a very narrow link between two conducting materials. Such a link can be formed by imposing a confining constriction in a wire or by forcing the electrons to pass through a narrow channel defined electrostatically when they are driven from one two- or three-dimensional region of the sample to the other. In the case of very narrow constrictions of width W, narrower than the mean free path and the phase coherence length ($W \ll l, L_\phi$), such a constriction is called ballistic quantum point contact. The conductance through ballistic quantum point contacts (see figure 8) was discovered [16, 15] to be quantized in units of $2e^2/h$. An overview on transport through ballistic point contacts and the connection to the quantum Hall effect can be found in reference [17].

Such experiments require typically sub-Kelvin temperatures for

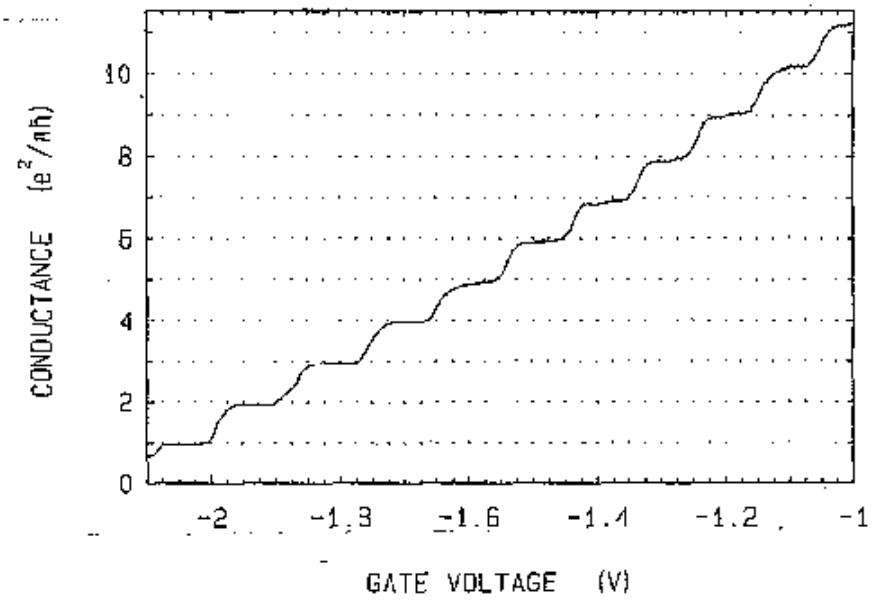

Figure 8: The conductance through a quantum point contact as a function of the gate voltage. The conductance exhibits clear steps of height $2e^2/h$ (from [15]).

constrictions of $W < 1\mu$m in two-dimensional electron gases defined in semiconductor heterostructures. However, it was recently shown [18] that the conductance quantization can be observed using an extremely simple setup. When two macroscopic metal wires touching each other are separated, the conductance of this contact decreases in quantized steps in the last fractions of milliseconds of the separation. These steps can be observed at room temperature using a fast oscilloscope. The contact region seems to be of atomic size before the contact is lost completely such that even the small phase coherence length at room temperature is large enough to observe the mesoscopic effect of the quantization of the conductance.

1.2.6 Persistent Currents in Mesoscopic Rings

Electrons in mesoscopic rings can support a current around the ring in thermodynamic equilibrium, even at zero temperature when only the many-body ground state is occupied. This current depends on the magnetic flux Φ piercing the ring and cannot decay dissipatively. It therefore flows forever even in normal conducting materials and this is why it is called persistent current. Persistent currents have been predicted in the early days of quantum mechanics by Hund [19], but

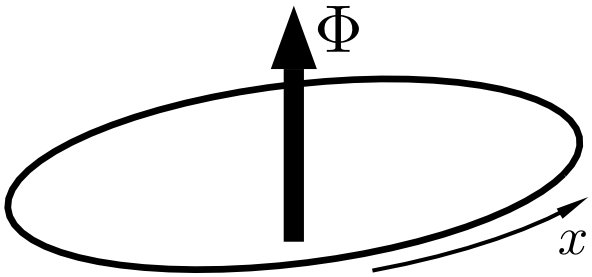

Figure 9: An ideal one-dimensional ring, pierced by the magnetic flux Φ.

their experimental relevance for mesoscopic systems has been recognized only much later [20]. For a detailed introduction see reference [1], for a review on theoretical aspects we refer the reader to reference [21].

Let us consider an ideal one-dimensional ring of circumference $L \ll L_\phi$, as shown in figure 9. It is well known that a magnetic field cannot affect the behavior of one-dimensional systems. This however does not hold when the one-dimensional system is closed to a ring. In this topology, the flux Φ threading the ring leads to a phase shift of $2\pi\Phi/\Phi_0$ accumulated by an electron traveling around the ring, $\Phi_0 = h/e$ being the flux quantum. Using a gauge transformation, this phase shift can be cast [22] into the boundary condition, eliminating the magnetic vector potential from the Schrödinger equation for the electrons and leading to generalized periodic boundary conditions

$$\psi(x = 0) = \exp(\mathrm{i}2\pi\Phi/\Phi_0)\psi(x = L) \tag{10}$$

for the one-particle wave-functions $\psi(x)$. This immediately implies that all the electronic properties of the ring must be periodic in the magnetic flux, the period being the flux quantum Φ_0, similar to the Aharonov-Bohm effect discussed in section 1.2.1.

The wave-functions of non-interacting electrons in a clean ring are plane waves

$$\psi(x) \propto \exp(\mathrm{i}kx)\,. \tag{11}$$

The boundary condition of equation (10) restricts the possible wave-vectors k to the values

$$k_n = \frac{2\pi}{L}\left(n - \frac{\Phi}{\Phi_0}\right) \tag{12}$$

with $n = \{0, \pm1, \pm2, \pm3, \ldots\}$. The flux-dependence of the correspond-

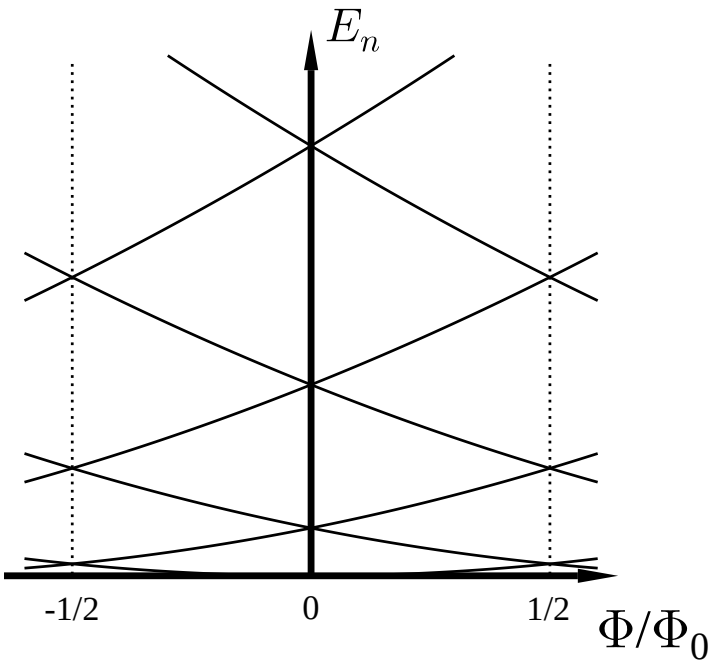

Figure 10: Flux dependence of the lowest one-particle energies in a ring, for $-3 \leq n \leq 3$ (see equation (13).

ing one-particle energies

$$E_n = \frac{\hbar^2 k_n^2}{2m} = \frac{1}{2m}\left[\frac{h}{L}\left(n - \frac{\Phi}{\Phi_0}\right)\right]^2 \tag{13}$$

is plotted in figure 10. The persistent current at zero temperature is then given by the sum of the currents $e\hbar k_n/mL$ of the lowest levels up to the electron number in the ring. The persistent current can be written as

$$I_{\mathrm{p}} = -\frac{\mathrm{d}E}{\mathrm{d}\Phi} \tag{14}$$

with the total energy of the electrons E. Since at a given value of Φ the sign of the derivatives of the one-particle energies with respect to the magnetic flux oscillates with the quantum number n, the total persistent current is diminished by cancelations of the contributions of adjacent levels. The resulting current $I_p^{\mathrm{1d,clean}}$ at large particle number is dominated by the last electron (at the Fermi level) and of the order of

$$I_p^{\mathrm{1d,clean}} \sim \frac{ev_{\mathrm{F}}}{L} \tag{15}$$

with the Fermi velocity v_{F}.

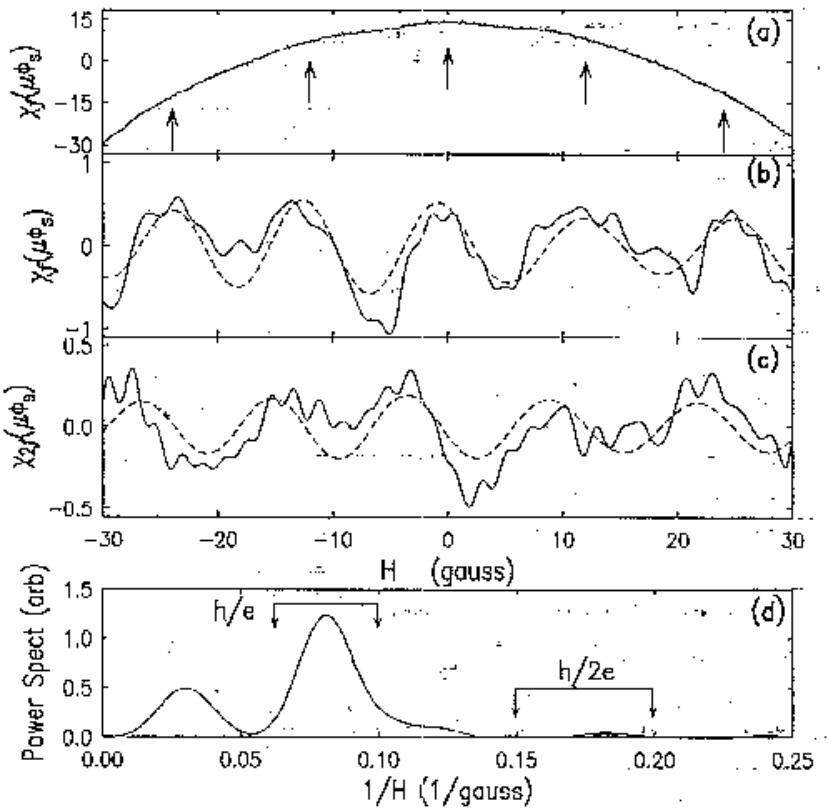

Figure 11: Experimental result for the magnetic field dependence of the magnetic susceptibility of a single disordered mesoscopic metal ring. (a): raw data, the arrows indicate the maxima of the h/e-oscillations. (b): after subtraction of the background signal. (c): differential signal consistent with (b). (d): Fourier transform confirming the period h/e of the flux dependence (from [23]).

In disordered rings of finite width with an elastic mean free path $l \ll L$, the theoretical value even for non-interacting electrons is much more difficult to obtain. In the diffusive regime, one expects [24, 25, 26] a persistent current of the order of

$$I_{\rm p}^{\rm diff} \sim \frac{ev_{\rm F}}{L}\,\frac{l}{L}\,, \tag{16}$$

which is reduced by a factor of l/L with respect to the clean case.

The experimental value of the persistent current in diffusive rings [27, 23] is however much larger (at least an order of magnitude) than this theoretical prediction. The discrepancy is believed to be due to the electron-electron interaction, which was neglected in the derivation

of equation (16). While the electron-electron interaction seems to play an essential role, the disorder in the sample is also important: Interactions cannot affect the persistent current in clean rotationally invariant 1d rings [28, 29, 30], and the non-interacting result (15) is consistent with the experimental one for a clean semiconductor ring in the ballistic regime [31].

This has generated a large theoretical activity, dealing with the combined effect of interactions and disorder on the enhancement of persistent currents in mesoscopic rings (for an overview see e.g. [32, 1, 21] and references therein). Even though different theoretical approaches suggest an increase of the persistent current in disordered samples due to repulsive Coulomb interactions, a quantitative understanding of the experiments is still lacking.

2 Theory of Electronic Transport in Mesoscopic Structures

In this section we introduce the reader to the theory of electronic transport in mesoscopic systems. After a presentation of the linear response formalism, we shall discuss the Landauer formalism in more detail and discuss a few applications of the approach to experimental situations. At the end, we will introduce to the concepts of resonant and sequential tunneling in double-barrier structures. For further reading on the theory of quantum transport, we recommend [2] and the recent book [3].

2.1 Breakdown of Classical Transport

Classically, the electrical conductance G of a block of a given material is described by

$$G = \frac{I}{V} = \sigma \frac{A}{L}, \tag{17}$$

the cross-section A and the length L containing the only form and size dependence and σ being the material-dependent conductivity. G is simply the inverse of the resistance. From Drude's theory [33] one gets

$$\sigma = e^2 n \tau_{\mathrm{s}} \tag{18}$$

with the charge density n and the momentum relaxation or scattering time τ_{s}. The size dependence of equation (17) implies the well known laws according to which the resistance of resistors in series is additive while the conductance is additive when the conductors are parallel in the circuit.

However, the description of electrical transport by equations (17) and (18) fails when the size of the system (longitudinal or lateral) becomes smaller than or comparable to the size of at least one of the following characteristic length scales:

- The Fermi wavelength λ_{F}. At this scale the quantum nature of the electrons dominates their behavior and classical descriptions fail.
- The mean free path $l = v_{\mathrm{F}} \tau_{\mathrm{s}}$. In metals it is often of the order of 10nm, while it can be as large as 100μm in extremely pure semiconductors at milli-Kelvin temperatures. Below this length scale, the transport becomes ballistic and the classical descriptions (which assume diffusive motion of the electrons) break down.

- The phase coherence length L_ϕ, which is essentially due to inelastic scattering and strongly temperature dependent. At this length scale, quantum mechanical interference effects appear and modify the classical behavior of the sample.

Since the classical description of electronic transport cannot be applied to individual samples in the mesoscopic regime, we present now approaches which take into account the quantum nature of the electrons and do not neglect quantum mechanical interference effects.

2.2 Linear Response Theory

Quantum mechanical linear response theory provides a general formalism for the calculation of the frequency dependent conductance of a quantum system. It allows to include the effect of a driving field and, at least in principle, to treat inelastic processes and interactions in mesoscopic systems in a systematic manner [34].

The linear response theory for the electrical conductivity is presented in numerous textbooks, e. g. in [35, 36]. However, in mesoscopic systems the electric field is varying over the spatial extension of the sample and geometrical confinement effects dominating the behavior destroy the translational invariance of the problem. This requires a non-standard form of the Kubo formula. We therefore derive the conductance formula needed for calculating the frequency dependent conductance of mesoscopic systems in linear response to an electric field, following references [37, 38].

We start from the Hamiltonian

$$H_{\rm tot} = H + H' \,, \tag{19}$$

where

$$H = \sum_i \left(\frac{1}{2m} \vec{p}_i^{\,2} + U(\vec{x}_i) \right) \tag{20}$$

describes the quantum system of non-interacting particles in the potential $U(\vec{x})$. The part H' takes into account the interaction with the electric field that is assumed to be infinitesimally weak and treated in lowest order. The sum runs over all the electrons in the system. e and m are the charge and the (effective) mass of the electrons, respectively. Expressing the electric field

$$\vec{E}(\vec{x},t) = -\frac{\partial \vec{A}(\vec{x},t)}{\partial t} \tag{21}$$

via the vector potential, we use the Coulomb gauge $\nabla \vec{A} = 0$ and set the electrostatic potential $\Phi = 0$. The current density operator can

be written in the form

$$\vec{j}(\vec{x}) = \frac{e}{2m} \sum_i \left[\vec{p}_i, \delta(\vec{x} - \vec{x}_i)\right]_+ , \tag{22}$$

where $[\ldots,\ldots]_+$ denotes the anticommutator. We have to mention that we have omitted a diamagnetic term which is of no importance for the dissipative conductance we are going to calculate. This form of the current density operator leads to the usual result for the matrix elements in space representation

$$\vec{j}_{ij}(\vec{x}) := \langle i \mid \vec{j}(\vec{x}) \mid j \rangle = \frac{e\hbar}{2\mathrm{i}m} \left(\psi_j(\vec{x}) \nabla \psi_i^*(\vec{x}) - \psi_i^*(\vec{x}) \nabla \psi_j(\vec{x})\right) \tag{23}$$

with the eigenfunctions of the unperturbed Hamiltonian ψ_i. The lowest order term in the vector potential entering the perturbing Hamiltonian is

$$H' = -\frac{e}{m} \sum_i \left(\vec{p}_i \vec{A} + \vec{A} \vec{p}_i\right) \tag{24}$$

and can be expressed as

$$H' = -\int d^3x \vec{A}(\vec{x}, t) \vec{j}(\vec{x}) \,. \tag{25}$$

To calculate the thermal expectation value of the current, we use the density operator ρ, whose time evolution is governed by the Liouville–von Neumann equation

$$\mathrm{i}\hbar \frac{\partial \rho}{\partial t} = [H_{\mathrm{tot}}, \rho] \,. \tag{26}$$

We assume adiabatic switching on of the perturbation by a monochromatic field

$$\vec{A}(\vec{x}, t) = \frac{\mathrm{i}}{\omega + \mathrm{i}\eta} \vec{E}(\vec{x}) e^{-\mathrm{i}(\omega + \mathrm{i}\eta)t} \,. \tag{27}$$

The (infinitesimal) imaginary part of the frequency $i\eta$ guarantees the vanishing of the electric field at $t \to -\infty$. Therefore, the appropriate initial condition at $t = -\infty$ for the solution of (26) is thermal equilibrium described by

$$\rho_0 = \sum_i f(E_i) \mid i \rangle \langle i \mid \,. \tag{28}$$

The eigenstates $\mid i\rangle$ are associated with the corresponding eigenenergies E_i of the unperturbed Hamiltonian H. We note

$$f(E) = \frac{1}{\exp[\beta(E - E_{\mathrm{F}})] + 1} \tag{29}$$

the Fermi–Dirac distribution function with the inverse temperature $\beta = 1/(k_{\mathrm{B}}T)$ and the Fermi energy E_{F}. Writing $\rho(t) = \rho_0 + \rho'(t)$, and keeping only terms linear in the perturbation, the Fourier transform of (26) gives

$$\hbar\omega\rho'(\omega) = [H, \rho'(\omega)] + [H'(\omega), \rho_0]\,. \tag{30}$$

Solving for $\rho'(\omega)$ in the basis of the unperturbed eigenstates, one finds the matrix elements

$$\rho'_{ij}(\omega) = \frac{f(E_j) - f(E_i)}{E_j - E_i + \hbar(\omega + i\eta)} H'_{ij}(\omega)\,. \tag{31}$$

The thermal expectation value for the current density is the trace over the current density operator weighted with the density operator

$$\langle\vec{j}(\vec{x}, t)\rangle = \mathrm{Tr}\left(\rho_0 j(\vec{x}, t)\right) + \mathrm{Tr}\left(\rho'(t) j(\vec{x}, t)\right)\,. \tag{32}$$

The first (equilibrium) term can be shown to vanish and the evaluation of the second one using (31) with (25) and (27) gives the result

$$\langle\vec{j}(\vec{x}, \omega)\rangle = \int d^3x' \tilde{\sigma}(\vec{x}, \vec{x}', \omega)\vec{E}(\vec{x}', \omega) \tag{33}$$

with the nonlocal, frequency–dependent conductivity tensor

$$\tilde{\sigma}(\vec{x}, \vec{x}', \omega) = (-\mathrm{i}) \sum_{i,j} \frac{f(E_j) - f(E_i)}{\omega + \mathrm{i}\eta} \frac{\vec{j}_{ij}(\vec{x})\vec{j}_{ji}(\vec{x}')}{E_j - E_i + \hbar(\omega + \mathrm{i}\eta)}\,. \tag{34}$$

This result containing two current density matrix elements representing a current–current correlation function can be interpreted in terms of electron–hole excitations created at x', propagating through the system and recombining at x. The dissipative conductivity can be defined using the density of absorbed power averaged over one period

$$p(\vec{x}, \omega) = \frac{\omega}{2\pi} \int_{t_0}^{t_0 + 2\pi/\omega} dt\, \vec{E}(\vec{x}, t)\langle\vec{j}(\vec{x}, t)\rangle\,. \tag{35}$$

Solely the real part of the conductivity contributes to the absorbed power. Thus, the dissipative conductivity is

$$\sigma(\vec{x}, \vec{x}', \omega) = \mathrm{Re}[\tilde{\sigma}(\vec{x}, \vec{x}', \omega)]\,. \tag{36}$$

For any finite frequency, the real part of (34) is given by

$$\sigma(\vec{x}, \vec{x}', \omega) = -\pi \sum_{i,j} \frac{f(E_j) - f(E_i)}{\omega} \vec{j}_{ij}(\vec{x})\vec{j}_{ji}(\vec{x}')\delta(E_j - E_i + \hbar\omega) \tag{37}$$

in the limit $\eta \longrightarrow 0$.

2.2.1 Definition of the Conductance

In order to determine the conductance, the spatial shape of the applied electric field has to be fixed. Then, the frequency dependent current can be calculated and related to the voltage drop. We now consider a quasi–one dimensional wire and an electric field is taken in the longitudinal direction described by the coordinate x ($\vec{x} = (x, x_\perp)$).

The conductance is defined via the absorbed power [38, 39, 40]

$$\Gamma(\omega) = \frac{2P(\omega)}{V^2}\,. \tag{38}$$

The energy absorption rate

$$P(\omega) = \frac{\omega}{2\pi} \int_{t_0}^{t_0+2\pi/\omega} dt \int dx\, E(x,t)\langle j(x,t)\rangle \tag{39}$$

is an average over one period $T = 2\pi/\omega$ of the driving field and the voltage is $V = \int \mathrm{d}x\, E(x)$.

Due to the presence of quantum coherence, the dc-limit of the conductance does not depend at all on the details of the external electric field and only the voltage drop between the reservoirs determines the current. In contrast, at finite frequencies, the conductance depends sensitively on the shape of the electric field. In addition, to evaluate the conductance using the linear response formalism, all the wavefunctions must be known explicitly. This information is often difficult to obtain, but linear response theory is rather systematic and general. We discuss in the next section the Landauer approach which is very useful and intuitive in the dc-limit, but difficult to generalize to finite frequencies or to systems of interacting particles.

2.3 The Landauer Approach

The approach of Landauer [41] (for a recent introduction see [2]) to the conductance of mesoscopic systems is particularly intuitive. It describes the conductance of a quantum system in terms of its scattering properties. The setup one has in mind is sketched in figure 12. The quantum system under consideration is connected to two reservoirs left and right of the system. The reservoirs are assumed to be macroscopic and in thermal equilibrium. They are therefore described by only two parameters, the temperature and the chemical potential. The difference between the chemical potentials μ_1 and μ_2 in the left and right reservoir is the applied voltage $eV = \mu_1 - \mu_2$. As connection between the reservoirs and the quantum system one assumes ideal

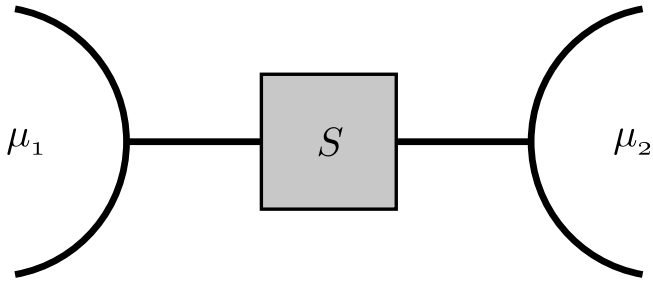

Figure 12: The idea of the Landauer approach to the conductance: A mesoscopic system is connected *via* ideal leads to reservoirs. The reservoirs are described by the chemical potentials μ_1 and μ_2. The conductance is expressed in terms of the scattering properties (scattering matrix S) of the system for the plane waves in the leads.

leads without any impurities or internal structure. These leads can be perfectly one-dimensional wires or quasi one-dimensional systems with a constant cross-section. The important property of the leads is that the electrons traveling within them are plane waves in longitudinal direction and suffer no backscattering whatsoever.

The properties of the quantum system are then described by its scattering matrix S in the basis of the plane waves inside the leads. If the dominant process is the reflection of an incoming wave back into the initial lead, the system is a poor conductor. If, in contrary, most of the incoming electrons are transmitted to the other reservoir, the conductance is large. Thus, the conductance of a quantum system is determined by its scattering properties.

2.3.1 One-Channel Two-Point Conductance

Let us consider the simplest case of perfect one-dimensional leads. Then, the propagating states that travel towards the quantum scatterer are $\propto a\exp(\mathrm{i}kx)$ in the left lead (moving rightwards) and $\propto b\exp(-\mathrm{i}kx)$ in the right lead (moving leftwards). The scattered electrons leaving the scatterer are described by the plane waves $\propto c\exp(-\mathrm{i}kx)$ in the left lead (moving leftwards) and $\propto d\exp(\mathrm{i}kx)$ in the right lead (moving rightwards). The amplitudes c and d of the scattered waves are related to the amplitudes of the incident waves by the scattering matrix S:

$$\begin{pmatrix} c \\ d \end{pmatrix} = S \begin{pmatrix} a \\ b \end{pmatrix} . \tag{40}$$

In the simple one-dimensional case, the scattering matrix can be written in the form

$$S = \begin{pmatrix} r & t' \\ t & r' \end{pmatrix} \tag{41}$$

with (in general complex) transmission and reflection amplitudes t, t' and r, r', respectively. The transmission and reflection probabilities are then given by $T = |t^2|$ and $R = |r^2|$, respectively. Since incident electrons must be either reflected or transmitted, probability conservation implies

$$T + R = 1\,. \tag{42}$$

More generally speaking, this is a consequence of current conservation which can be written as

$$\left| \begin{pmatrix} c \\ d \end{pmatrix} \right|^2 = \left| \begin{pmatrix} a \\ b \end{pmatrix} \right|^2 . \tag{43}$$

This is equivalent to the requirement of an unitary scattering matrix S (fulfilling $SS^+ = 1$). In the case of time reversal and spin rotation symmetry, more restrictions on the scattering matrix exist which require S to be a symmetric matrix. For the matrix of equation (41), the requirements can be fulfilled by choosing t and r real, $t' = t$ and $r' = -r$.

The current flowing from the left to the right reservoir can then be calculated as the density of electrons in the left lead $2\rho(E)f_1(E)$ times the current $ev(E)T(E)$ carried into the right reservoir at the same energy, integrated over all energies, yielding

$$I_{1\to 2} = 2\int_0^\infty \mathrm{d}E\, \rho(E) f_1(E)\, ev(E) T(E)\,. \tag{44}$$

Here, the prefactor 2 takes into account the spin degree of freedom and

$$\rho(E) = \frac{\sqrt{m/2E}}{h} \tag{45}$$

is the energy dependent density of states for one spin direction in a one-dimensional system. The occupation probability of these states is described by the Fermi-Dirac distribution

$$f_1(E) = \frac{1}{1 + \exp[(E - \mu_1)/k_\mathrm{B}T]}\,. \tag{46}$$

Note that there is no Pauli-blocking factor $(1 - f_2(E))$ in equation (44), taking into account the occupation of the states in the right reservoir. This is because the states carrying the current are coherent scattering states which are extended through the whole system, being

filled by the left reservoir. This of course breaks down in the presence of dissipation [42] causing phase breaking processes while electrons travel from one reservoir to the other. The energy dependence of the velocity of an electron in one dimension is given by

$$v(E) = \sqrt{2E/m}\,, \tag{47}$$

while the transmission probability $T(E)$ remains the only system-dependent property in equation (44).

Plugging the expressions (45) and (47) for the density of states and the velocity of the electrons in the leads into equation (44), the energy and mass dependences of the density and the velocity cancel each other and one obtains

$$I_{1\to 2} = \frac{2e}{h}\int_0^\infty \mathrm{d}E\, f_1(E)T(E)\,. \tag{48}$$

By symmetry, the current flowing from the right to the left lead is given by

$$I_{2\to 1} = \frac{2e}{h}\int_0^\infty \mathrm{d}E\, f_2(E)T(E) \tag{49}$$

and the total current can be obtained from the difference

$$I = I_{1\to 2} - I_{2\to 1} = \frac{2e}{h}\int_0^\infty \mathrm{d}E\, T(E)(f_1(E) - f_2(E))\,. \tag{50}$$

In the case of low temperature, the Fermi-Dirac distributions (46) can be approximated by a step function $f_i(E) \approx \Theta(\mu_i - E)$ and the resulting integral is restricted to the vicinity of the Fermi energy E_F at low voltage $V = (\mu_1 - \mu_2)/e \to 0$. In these limits, the integral in (50) can be evaluated and one obtains the current

$$I = \frac{2e^2}{h} V T(E_\mathrm{F}) \tag{51}$$

and the conductance

$$G = \frac{2e^2}{h} T(E_\mathrm{F})\,. \tag{52}$$

Equation (52) is the so-called one-channel two-point Landauer formula.

Some years ago, there have been intensive discussions whether or not in the genuine four-probe Landauer formula [41, 43]

$$G = \frac{2e^2}{h}\,\frac{T}{1-T} \tag{53}$$

the denominator should be used. The different formulas were found to correspond to different experimental setups [44]. While the four-probe

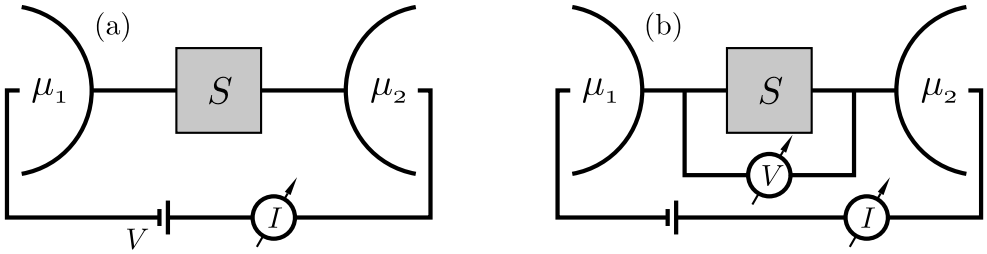

Figure 13: Two-probe setup (a) *versus* four-probe setup (b). In the two-probe case, the voltage is taken in the reservoirs yielding $V = (\mu_1 - \mu_2)/e$. In the four-probe case, the voltage is measured in the leads immediately before and after the scatterer.

formula describes a conductor connected via ideal one-dimensional leads to reservoirs and the voltage is measured across the sample without the leads (figure 13, right), the two-probe formula (52) corresponds to measuring both, voltage and current via contacts well inside the reservoirs (figure 13, left).

The four-probe Landauer formula (53) has never been justified by a decent linear response calculation. In contrast, the two-probe version (without the denominator $1-T$) is recovered by the dc–limit of linear response theory. This can be shown for very general situations [37]. Experimentally, it is practically impossible to measure the voltage difference in the leads directly before and after the sample without disturbing the phase coherence of the transport between the reservoirs [45]. We therefore concentrate on the two-probe version of the formula in the following.

Let us consider a perfect one-dimensional conductor with transmission probability $T = 1$. In this case, the two-probe Landauer formula (52) yields the conductance

$$G = \frac{2e^2}{h}\,, \tag{54}$$

corresponding to a finite resistance of $h/2e^2$, half of the resistance quantum

$$\frac{h}{e^2} \approx 26\mathrm{k}\Omega \tag{55}$$

arising per spin direction. The question where this resistance comes from and how a perfect conductor can have a finite resistance has lead to controversial discussions [46]. Since no backscattering inside the ideal one-dimensional conductor is taken into account, this resistance arises solely from the contact resistance between the reservoirs and the ideal wire. For a more detailed discussion, see [1].

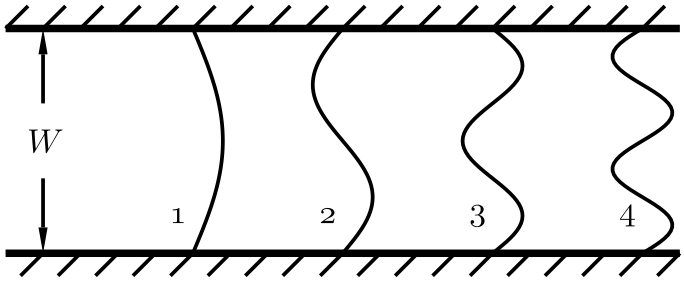

Figure 14: Two-dimensional lead of width W. The transverse modes are quantized by the lateral confinement.

2.3.2 Multi-Channel Two-Point Conductance

A more realistic situation is the one of quasi one-dimensional leads of finite cross-section connecting the quantum scatterer to the reservoirs. We discuss now the simplest example of a two-dimensional strip along the x-axis having the width W in y-direction, as sketched in figure 14. Assuming a perfect lead, the confinement potential

$$U(x, y) = U(y) \tag{56}$$

only depends on the transverse coordinate y. Then, the Schrödinger equation

$$-\frac{\hbar^2}{2m}\Delta\psi(x, y) + U(y)\psi(x, y) = E\psi(x, y) \tag{57}$$

can be separated and one gets as solutions the product wave functions

$$\psi(x, y) \propto \exp(\mathrm{i}kx)\phi_n(y) \tag{58}$$

and the corresponding energies

$$E_{k,n} = \frac{\hbar^2 k^2}{2m} + E_n\,, \tag{59}$$

where the $\phi_n(y)$ and E_n are the one-dimensional eigenfunctions and the eigenenergies, respectively, of confined particles in the transverse potential $U(y)$. The longitudinal part, in contrast, reflects free propagation with wave-number k along the x-direction. The quantized transverse parts of the wave-functions are analogous to the electromagnetic modes in wave-guides and are called channels or transverse modes in this context.

The dispersion relation (59) exhibits several branches, one per transverse quantum number n. Each branch is equivalent to an ideal one-dimensional system except for the energy offset E_n. Neglecting

the interaction between the electrons, the total zero-temperature current through a quantum scatterer which is connected to reservoirs by multi-channel leads is then a sum over all occupied channels in the left and right lead

$$G = \frac{2e^2}{h} \sum_{n,m} T_{n,m} \,, \tag{60}$$

with $T_{n,m}$ being the probability of an incoming electron in channel n in the left lead to be transmitted to the channel m in the right lead. Equation (60) is called the multi-channel two-probe Landauer formula. Note that the sum runs only over occupied channels with $E_n, E_m < E_\mathrm{F}$, since channels with an offset energy above the Fermi energy cannot contribute to the transport.

It is instructive to consider a perfect quasi one-dimensional conductor with

$$T_{n,m} = \delta_{n,m} \tag{61}$$

for which each channel is perfectly transmitted and no scattering from one channel to another is allowed. Then, the sum in equation (60) reduces to the number of occupied channels N_c with an offset energy E_n lower than the Fermi energy and one gets the conductance

$$G = \frac{2e^2}{h} N_\mathrm{c} \tag{62}$$

of a quantum wire. This conductance is quantized in units of $2e^2/h$. Since the offset energies E_n increase when the width of the wire W is reduced, the conductance of a quantum wire is expected to vary in steps of $2e^2/h$ when the width is changed. This is an important ingredient for the understanding of the conductance quantization in quantum point contacts (see section 1.2.5).

For the description of the currents in more complicated setups with more than two reservoirs, a generalization of the two-terminal two-point Landauer formula to multi-terminal devices was derived by Büttiker [47].

2.3.3 Edge States and Quantum Hall Effect

The Landauer concept of formulating the phase coherent transport in a mesoscopic sample is very useful for explaining the electronic behavior of a variety of systems including quantum wires and quantum point contacts. Its application to a two-dimensional electron in a strong perpendicular magnetic field is also very instructive and plays an important role in the understanding of the quantum Hall effect (see section 1.2.2).

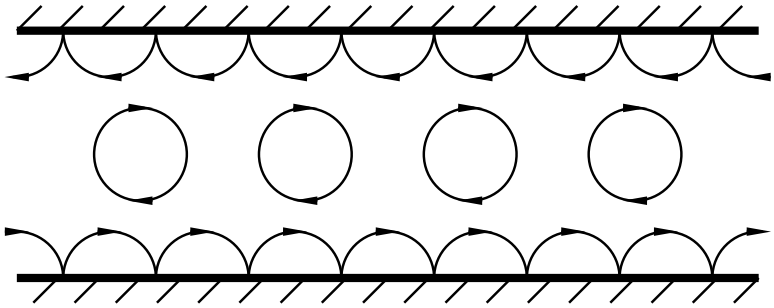

Figure 15: Classical trajectories of electrons in a strong magnetic field. Localized cyclotron orbits occur in the bulk of the sample. At the edges of the sample, skipping orbits lead to a propagation of the electrons along the edge.

As discussed in section 1.2.2, the strong magnetic field leads to the formation of Landau levels. One picture for explaining features of the quantum Hall effect invokes the presence of a small impurity concentration in the sample [48, 1]. This leads to a small broadening of the Landau levels with strongly localized states in the tails and contributions to a finite current only in the center of the Landau level. While this helps to explain the finite width of the Hall resistance, another more intuitive picture has been developed, according to which the edges of the sample play a crucial role for the currents flowing in the quantum Hall effect (for a review see [49], for an introduction [2]). This is the so-called edge-state picture we will briefly present in this section.

It is instructive to consider the classical trajectories of electrons moving in a clean sample subject to a strong magnetic field. They are drawn schematically in figure 15. In the bulk of the sample, the classical trajectories are closed cyclotron orbits which cannot contribute to the transport through the sample. In contrast, the trajectories near the edges of the sample are reflected there and one immediately realizes the fundamental difference: On the resulting so-called skipping orbits, the electrons travel along the edges, thereby leading to a finite current flowing through the sample. In a quantum mechanical picture, the breaking of the translational symmetry by the consideration of the finite size of the sample modifies the Landau levels. States localized close to the edges correspond to higher energies than the unmodified states in the bulk which are still described by equation (7). Therefore, even when the Fermi energy lies between two Landau levels, the part close to the edge which is bent upwards crosses the Fermi energy and gives rise to edge channels. There, an electron staying close to

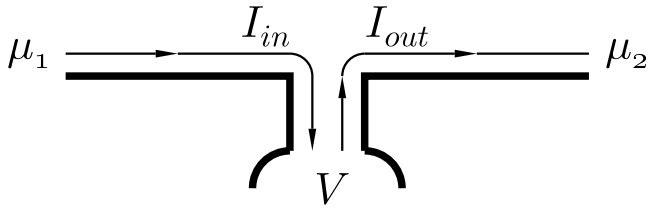

Figure 16: A voltage probe. The edge channels coming from the left hand side enter the probe while the channels leaving the probe travel to the right hand side.

the edge can travel through the sample. However, as suggested by the skipping orbits, an edge channel can support only current in one direction, determined by the orientation of the magnetic field. The channels at the opposite edge support current flowing to the other direction.

Since exactly one edge channel per Landau level and spin is formed (provided the Fermi energy is above the bulk Landau level energy), the number of occupied Landau levels gives directly the number of channels carrying current along the edges. When the width W of the sample is much larger than the cyclotron radius $r_{\rm c}$ (this is well fulfilled at strong magnetic field in not too narrow samples), the overlap between edge channels corresponding to opposite sides of the sample and therewith the backscattering is exponentially suppressed. This means that an electron which starts to travel along an edge channel is transmitted through the sample and never reflected. Therefore, edge channels in the quantum Hall effect regime are perfect ballistic channels with transmission $T = 1$. The multi-channel Landauer formula (62) for an ideal wire can be applied with the number $N_{\rm c}$ of channels being given by the number of occupied Landau levels.

A voltage probe attached to one side of the sample is drawn schematically in figure 16. In this example, the current $I_{\rm in}$ of electrons entering the voltage probe comes exclusively from the left where the electrons have left a reservoir with chemical potential μ_1. The current $I_{\rm out}$ of electrons leaving the voltage probe goes to the right where the electrons enter the other reservoir with chemical potential μ_2.

Now, the voltage probe can itself be considered as a reservoir where the chemical potential μ_V is adjusted such that the net current flow $I_{\rm in} - I_{\rm out}$ vanishes. The resulting chemical potential determines the measured voltage $V = \mu_V/e$. Since the edge channels support current in only one direction, the current in the edge channels depends only

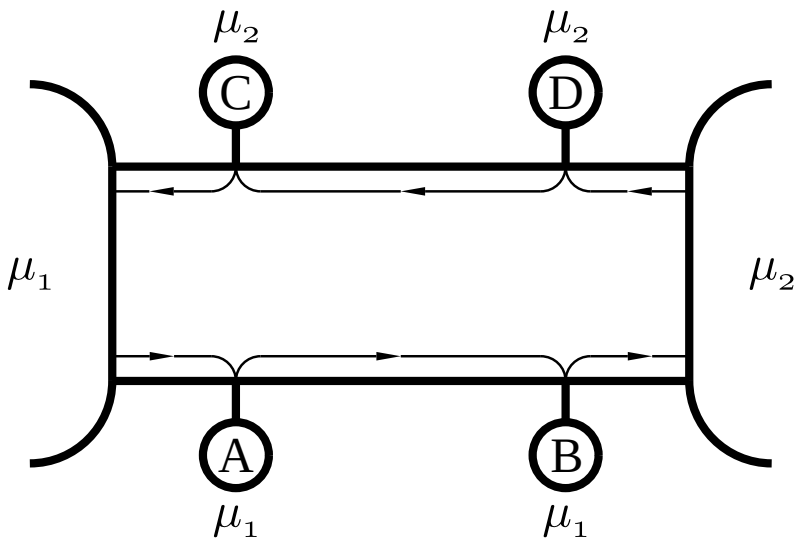

Figure 17: Hall geometry with the voltage probes A, B, C, and D. Due to the edge channel directions, A and B see the chemical potential μ_1 while the probes C and D give μ_2.

on the chemical potential of the reservoir in which they start. There is no dependence on the chemical potential of the reservoir towards which they are traveling. Thus, for the example of figure 16, one has

$$I_{\rm in} = I(\mu_1) \qquad \text{and} \qquad I_{\rm out} = I(\mu_V)\,, \tag{63}$$

implying immediately $\mu_V = \mu_1$. Therefore, all the voltage probes on the same side of the sample measure the same chemical potential which is determined by the reservoir where the edge channel starts.

In a Hall measurement (see figure 17), this means that the chemical potentials measured by the voltage probes A and B is μ_1 and the chemical potential measured at C and D is μ_2. Therefore, the longitudinal voltage drop

$$V_x = V_{\rm A} - V_{\rm B} = 0 \tag{64}$$

vanishes while the Hall voltage measured across the sample is given by

$$V_{\rm H} = V_{\rm A} - V_{\rm C} = \frac{\mu_1 - \mu_2}{e}\,. \tag{65}$$

The longitudinal current carried by the edge states is obtained from the ideal ballistic wire Landauer formula to

$$I_x = \frac{2e^2}{h}\, N_{\rm c}\, \frac{\mu_1 - \mu_2}{e}\,. \tag{66}$$

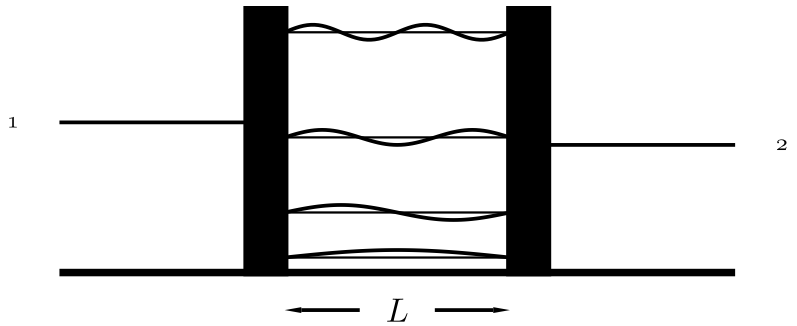

Figure 18: Sketch of a double barrier structure. Without interaction, the electrons in the leads are characterized by the chemical potentials μ_1 and μ_2, while quasi-bound states are formed between the barriers.

From equations (64), (65), and (66), one gets the longitudinal and the Hall resistance

$$R_x = \frac{V_x}{I_x} = 0 \qquad \text{and} \qquad R_{\mathrm{H}} = \frac{V_{\mathrm{H}}}{I_x} = \frac{h}{2e^2}\frac{1}{N_{\mathrm{c}}}\,, \tag{67}$$

describing essential features of the quantum Hall effect like the value of the Hall resistance plateaus and the vanishing of the longitudinal resistance. The high metrological precision of the measured Hall voltage and the independence of its values on the sample geometry can be traced back to the suppression of backscattering due to the spatial separation of the edge channels carrying current in opposite directions.

For further introductory reading, we recommend reference [2]. For a review on the importance of edge states and experimental aspects see reference [49].

2.4 Resonant *versus* Sequential Tunneling

The aim of this section is to introduce to the concepts of resonant and sequential tunneling. For this purpose, we use the example of a one-dimensional double-barrier structure as sketched in figure 18. In such a device, two different regimes exist, the regime of resonant tunneling and the regime of sequential tunneling (for further reading, we recommend reference [2]).

2.4.1 Resonant Tunneling

If we neglect the Coulomb interaction and assume that the transport through a double-barrier structure like in figure 18 is fully phase-

coherent, the conductance predicted by the Landauer formula is given by

$$G = \frac{2e^2}{h} \sum_{n,m} T_{n,m}(E_{\mathrm{F}}) \,, \tag{68}$$

where $T_{n,m}$ is the total transmission amplitude through the two barriers. Assuming that the lateral confinement potential of the quantum wire is independent of the barrier potential, the channels are not mixed and from a straightforward effectively one-dimensional calculation based on the matching of wave-functions, one obtains

$$T_{n,m}(E) = \delta_{n,m} \, \frac{T_1 T_2}{1 + R_1 R_2 - 2\sqrt{R_1 R_2} \cos\theta} \tag{69}$$

with $\theta = 2k(E)L + \theta_0$ where T_1 (T_2) and R_1 (R_2) are the transmission and reflections probabilities, respectively, of the left (right) barrier. L denotes the distance between the barriers, $k(E)$ the longitudinal component of the wave-vector corresponding to the energy E and θ_0 is an offset angle depending on the phases of the reflection amplitudes of the barriers.

Maxima in the transmission and therefore in the conductance occur at energies where $\cos\theta = 1$ or $2kL + \theta_0 = 2\pi n$. This is the quantization condition for bound states in a one-dimensional box of length L. Thus, the spectral properties of confined electrons can be probed by a transport experiment.

At these energies with $\cos\theta = 1$, the total transmission $T > T_1 T_2$ in larger than the product of the transmission probabilities of the two barriers. For a symmetric structure with $T_1 = T_2$, one obtains even perfect transmission $T = 1$ at the energies of quasi-discrete states between the barriers. This is called resonant tunneling and is based on the phase coherence during the entire process and the existence of scattering states through the whole structure. An optical analog is the well-known Fabry-Perot interferometer. The line-form of these resonances is Lorentzian with width $\gamma = \gamma_1 + \gamma_2$, where

$$\frac{\gamma_i}{\hbar} = \frac{v}{2L} \, T_i \tag{70}$$

is the escape rate through the barrier i. Thus, the natural line-width is given by the lifetime of the quasi-discrete states in the quantum dot. The resonant tunneling peaks can be resolved only when the width γ is smaller than their separation, the level spacing Δ. This requires barriers of low transmission. For more details on resonant tunneling see reference [2].

2.4.2 Sequential Tunneling

When the tunnel barriers are high and/or thick, the transmission probabilities and the escape rates (70) become very small. Then, the typical time an electron spends in the quantum dot

$$\tau_{\mathrm{D}} = \frac{\hbar}{\gamma} = \frac{2L}{v}\frac{1}{T_1 + T_2} \tag{71}$$

can become very long. However, the phenomenon of resonant tunneling is based on the phase coherence of the entire process and therefore restricted to the regime

$$\tau_{\mathrm{D}} \ll \tau_\phi \,. \tag{72}$$

In the opposite regime, when

$$\tau_{\mathrm{D}} \gg \tau_\phi \,, \tag{73}$$

the phase coherence is broken while the electron is inside the quantum dot. This regime is called the regime of sequential tunneling since the events can be ordered in time:

1. An electron tunnels from the left lead to the dot
2. The phase coherence is broken
3. An electron tunnels from the dot to the right lead

In this case, no coherent scattering states extended from the left lead throughout the dot region until the right lead exist. Nevertheless, it should still be possible to detect the quasi-discrete levels inside the dot if the time scales mentioned above are much longer

$$\tau_{\mathrm{D}} \gg \tau_\phi \gg \tau_{\mathrm{H}} = \frac{\hbar}{\Delta} \tag{74}$$

than the Heisenberg time τ_{H} related to the level spacing in the dot.

In this situation, a Pauli master equation for the occupation probabilities f_r of the quasi-discrete levels r at energies ϵ_r can be justified [50]. Still neglecting the Coulomb interaction between the electrons, one writes the current between the left reservoir (with chemical potential μ_1) and the level r of the dot as

$$I_{1\to r} = \frac{2e}{\hbar}\gamma_1 \left(f_1(\epsilon_r)(1-f_r) - f_r(1-f_1(\epsilon_r))\right) = \frac{2e}{\hbar}\gamma_1 \left(f_1(\epsilon_r) - f_r\right) . \tag{75}$$

In the same way, one expresses the current between the right lead (at chemical potential μ_2) and the level r as

$$I_{2\to r} = \frac{2e}{\hbar}\gamma_2 \left(f_2(\epsilon_r) - f_r\right) \tag{76}$$

and uses the current conservation in the static solution ($\partial f_r/\partial t$) to require

$$I_{1\to r} + I_{2\to r} = 0\,. \tag{77}$$

This allows to determine the occupation probability

$$f_r = \frac{\gamma_1 f_1(\epsilon_r) + \gamma_2 f_2(\epsilon_r)}{\gamma_1 + \gamma_2} \tag{78}$$

of the level r. The current flowing from the left to the right reservoir through the quantum dot is equal to the current from one of the reservoirs to the dot

$$I_{1\to r\to 2} = I_{1\to r} = -I_{2\to r}\,. \tag{79}$$

Plugging the occupation probability (78) into the expression (75) for the current, and summing over all levels r, one obtains the total current through the quantum dot

$$I_{1\to r\to 2} = \sum_r \frac{2e}{\hbar}\frac{\gamma_1\gamma_2}{\gamma_1+\gamma_2}\left(f_1(\epsilon_r) - f_2(\epsilon_r)\right)\,. \tag{80}$$

This gives maxima of the current at the same energies as the scheme of resonant tunneling. However, the line-form of the peaks is now determined by the thermal broadening of the step in the Fermi-Dirac distributions $f_{1/2}$ which describe the occupation of the electronic levels in the reservoirs.

3 Effects of the Electron-Electron Interaction

While a variety of phenomena can be understood within a (weakly interacting) quasi-particle approach, the always present strong Coulomb interaction between electrons can have a dramatic influence on the transport properties when the electrons are confined in low-dimensional systems. A prominent example is the Coulomb blockade effect and the resulting conductance oscillations in the transport through quantum dots [51]. The reduced dimensions are expected to render electronic correlations more important than in the bulk. Going to lower dimensions and/or very dilute limits results in a poorer screening of the electron-electron interaction, enhancing the role of Coulomb repulsions.

3.1 The Coulomb Blockade

Let us start with the example of a small tunnel junction, a potential barrier in a quantum wire between two well-conducting regions. According to the Landauer formula (60), the current should grow linearly with the applied voltage. However, in tunnel junctions with a very small cross section, measured in series with a large resistance, a suppression of the linear conductance and the appearance of a voltage offset in the current–voltage characteristics is observed [52] (see figure 19). In this experiment, an $\mathrm{Al/Al}_x\mathrm{O}_y\mathrm{/Al}$ junction with an area $A < 0.01\mu\mathrm{m}^2$ and an effective oxide layer thickness of about $d/\epsilon_\mathrm{r} = 0.15\mathrm{nm}$ was investigated at low temperature $T = 1\mathrm{K}$.

Considering that the junction also acts as a capacitor, such a small area of the junction corresponds to an extremely low capacity. Using the formula for a parallel-plate capacitor, one gets

$$C = \epsilon_0 \epsilon_\mathrm{r} \frac{A}{d} \approx 0.5\mathrm{fF} = 5 \times 10^{-16}\mathrm{F}\,. \tag{81}$$

The energy corresponding to the charging of a capacitor having such a small capacitance with one single electron

$$E_C = \frac{e^2}{2C} \tag{82}$$

is then approximately $300\mu e\mathrm{V}$. This corresponds to $k_\mathrm{B}T$ for a temperature of about 30K and thus represents an important energy scale in the problem. The charging energy is a consequence of the Coulomb interaction between the electrons and influences the transport properties of the tunnel junction in the following way.

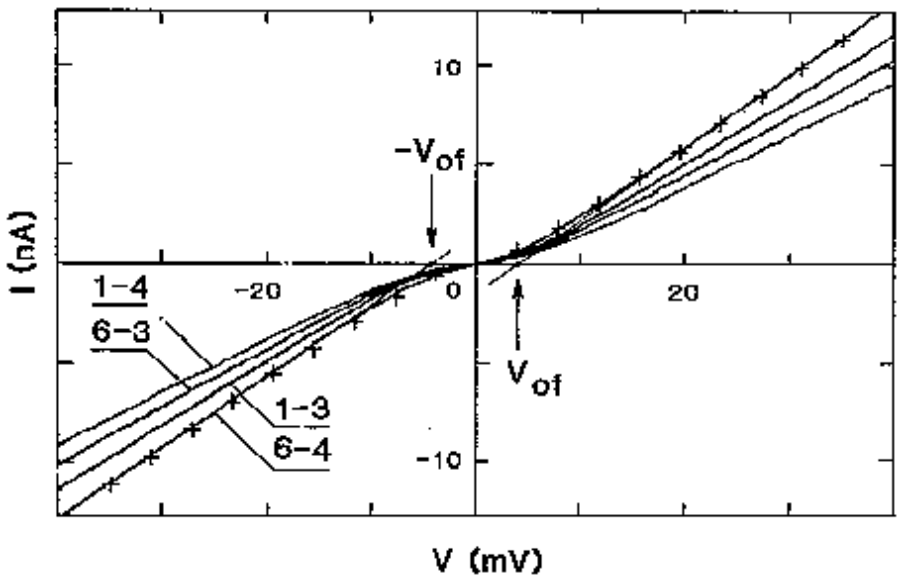

Figure 19: The current-voltage characteristics of samples containing low-capacitance tunnel junctions in series with more tunnel junctions providing a highly resistive environment. The offset voltage and the suppression of the linear conductance characteristic of the Coulomb blockade are clearly observed (from [52]).

Even though the charge

$$Q = CV \tag{83}$$

induced by the voltage V on the capacitor does not need to be an integer multiple of the elementary charge e, the tunneling of an electron through the barrier changes this charge by exactly one elementary charge. Immediately after the tunneling event, the charge on the capacitor is

$$Q' = Q - e\,. \tag{84}$$

The electronic transport is based on tunneling through the barrier and since tunneling conserves energy, these processes are suppressed when the energy needed to change the charge on the capacitor exceeds the available energy. Denoting the one-particle energy of the electron ϵ_1 and ϵ_2 before and after the tunneling, respectively, energy conservation requires

$$\epsilon_1 + \frac{Q^2}{2C} = \epsilon_2 + \frac{(Q-e)^2}{2C}\,. \tag{85}$$

Replacing Q by the voltage according to equation (83) and writing the voltage V in terms of the chemical potential difference $\mu_1 - \mu_2$,

one gets

$$\epsilon_1 - \epsilon_2 + \mu_1 - \mu_2 = \frac{e^2}{2C} = E_C \,. \tag{86}$$

Since at low temperature the energy of the electron before tunneling is below the chemical potential $\epsilon_1 \leq \mu_1$ and the energy after tunneling is above the other chemical potential $\epsilon_2 \geq \mu_2$, one has always $\epsilon_1 - \epsilon_2 \leq \mu_1 - \mu_2$ and obtains from (86) the condition for tunneling

$$2eV = 2(\mu_1 - \mu_2) \geq E_C \,. \tag{87}$$

This is the origin of the suppression of the linear conductance through ultra-small capacitances and explains the voltage offset

$$V_{\rm of} = \frac{E_C}{2e} \tag{88}$$

in the current-voltage characteristic of figure 19. This suppression of the conductance is a consequence of the granular structure of electronic charge combined with electron–electron interactions. It is called the Coulomb blockade effect and can lead to single electron tunneling as proposed in references [53, 50] (for introductions, see references [54, 55]). For a recent review, see chapter 3 of reference [3].

In order to be able to observe the Coulomb blockade effect, two main conditions must be fulfilled:

- Thermal fluctuations should be small enough in order not to provide the charging energy. This requires

  $$E_C \gg k_{\rm B}T \,, \tag{89}$$

  a condition which can be fulfilled in ultra-small capacitance junctions at low temperatures.

- Quantum fluctuations should be smaller than the charging energy. For a systematic treatment of this limitation, see [56]. According to a rough estimate, the energy uncertainty is due to the time τ it takes to restore the initial equilibrium charge Q on the capacitor. If this time is short, the energy uncertainty smears out the charging energy. Thus,

  $$E_C \gg \Delta E = \hbar/\tau \tag{90}$$

  must be fulfilled. If one estimates the time scale from the exponential decay of the capacitor charge in a classical RC circuit, $\tau \approx RC$, this results in the requirement to have a resistance of

  $$R \gg \frac{1}{\pi}\,\frac{h}{e^2} \tag{91}$$

in series. This is realized for small metal grains connected via tunnel barriers to the reservoirs and lead to the first observation of single electron charging and the Coulomb blockade effect [57]. In a controlled fabrication of artificial structures, using several small-area tunnel junctions, the single electron charging effects were first obtained in reference [58]. The Coulomb blockade becomes more pronounced when more tunnel junctions are put in series [52].

3.2 Transport through Quantum Dots

Since the conditions for observing the effects of single electron tunneling require a large resistance in series with the small-capacitance tunnel junction, it is most promising to study two tunnel junctions in series, separated by a very short distance (see the sketch in figure 18). In the region between the barriers, the electrons are confined and a quantum dot is formed which is only weakly connected to the exterior world by tunnel barriers.

The conductance through a quantum dot in the regime of sequential tunneling was dealt with in section 2.4.2, neglecting electron–electron interactions. Real electrons however do interact, and the addition of an electron to the quantum dot costs not only the one-particle energy ϵ_r, but also the electrostatic charging energy given by the repulsion of the electrons which are already there. This interaction dominates over the one-particle energy in the case of small dots and low electron density and strongly influences the transport properties of the quantum dots.

Including the charging energy as a constant E_C into the master equation description is called the orthodox theory of single electron tunneling in the literature [50, 59, 3].

The single-particle picture used above breaks down when electronic correlations in the quantum dot become important. This somewhat complicates the orthodox theory, but it is nevertheless possible to generalize it. One now has to deal with many-body states in the quantum dot and considers the occupation probabilities of these many-body levels [59]. The main difference is that the single particle energy levels ϵ_r are replaced by the energy

$$\mu_{\mathrm{D}}(N) = E_{N+1} - E_N \tag{92}$$

needed to add an electron to the dot containing N electrons. Here E_N stands for the many-body energy of N confined interacting electrons inside the quantum dot. Conductance peaks are expected when the Fermi energy is equal to the $\mu_{\mathrm{D}}(N)$ which corresponds to the energy

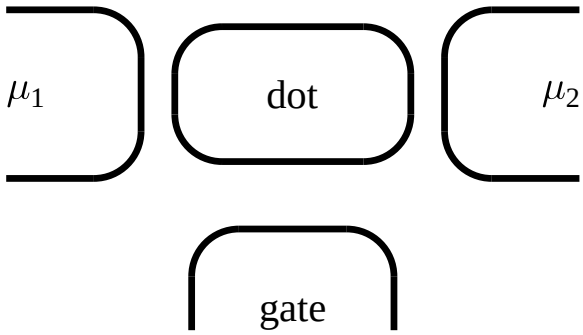

Figure 20: Sketch of a single electron transistor. Applying a voltage to the additional gate allows to control the electrostatic potential of the quantum dot. Note that the leads are connected to the dot through tunnel barriers while the gate is isolated and coupled only capacitively to the dot region.

difference between the many-body ground states in the dot. Then, single charge tunneling and the Coulomb blockade occur as discussed in section 3.1.

3.3 The Single Electron Transistor

The single electron transistor consists of a small quantum dot, connected weakly to leads, very much like the double barrier structure sketched in figure 18. The important additional feature is a side or back gate (see the sketch in figure 20) which allows to tune the electrostatic potential in the quantum dot. Such a setup can be formed in disordered quantum wires with a lateral gate where the dot appears between two accidentally close impurities [61]. A more controlled way to produce a single electron transistor is to use artificially fabricated semiconductor [60] or metallic [55] nanostructures where the size of the dot can be controlled. One of the main features of the behavior of such a single electron transistor is the appearance of conductance oscillations as a function of the gate voltage [60] (see figure (22). Qualitatively, this is expected from the discussion of resonant and sequential tunneling in double-barrier structures since the gate voltage allows to modify the one-particle energies in the quantum dot. As compared to the non-interacting theory, however, important differences appear. The spacing of the conductance peaks is larger than expected from the non-interacting theory, especially for small quantum dots. In addition, the conductance oscillations are very regular. This is due to the charging energy which dominates the energy nec-

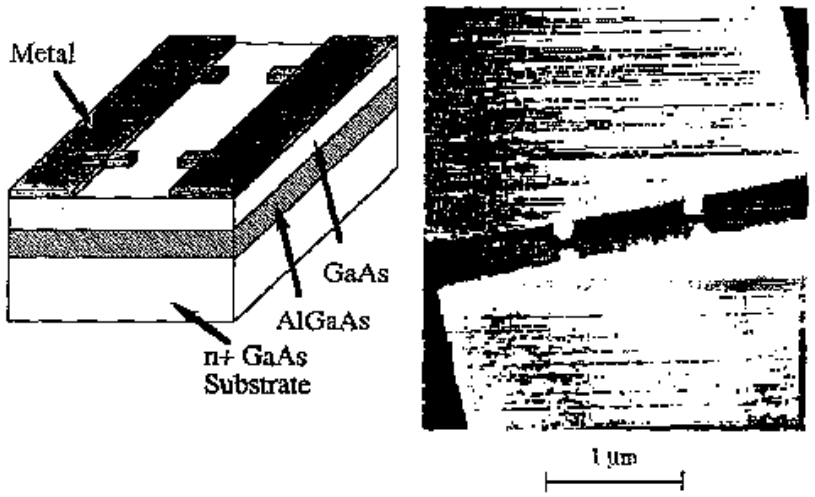

Figure 21: A single electron transistor device using the two-dimensional electron gas formed in a semiconductor heterostructure, here GaAs/GaAlAs. Negative voltage is applied to the metallic top gates, depleting the two-dimensional electron gas underneath. The fingers in these top gates lead to tunnel barriers in the effective potential landscape for the electrons. The overall electrostatic potential can be influenced via a back gate voltage V_g, applied to the substrate of the sample. Right: Top view of the device (from [60]).

essary to add an electron to the dot. The more irregular one-particle spectrum is of minor importance for this energy.

For an introduction to single electron transistors, we recommend reference [62]. For a discussion of the theoretical description of the behavior of the single electron transistor in the regime of sequential tunneling see reference [63].

3.3.1 Transport Spectroscopy

The nonlinear transport properties of quantum dots can be used to measure the addition spectrum of the confined electrons [64, 65, 66]. That the electronic correlations induced by the Coulomb interactions between the electrons in a quantum dot can have drastic consequences on its transport properties is illustrated by the spin blockade effect [67, 68, 69, 63] where the spin selection rules affecting the tunneling matrix elements together with the electronic correlations can lead to spectacular consequences like negative differential resistances and the suppression of conductance peaks.

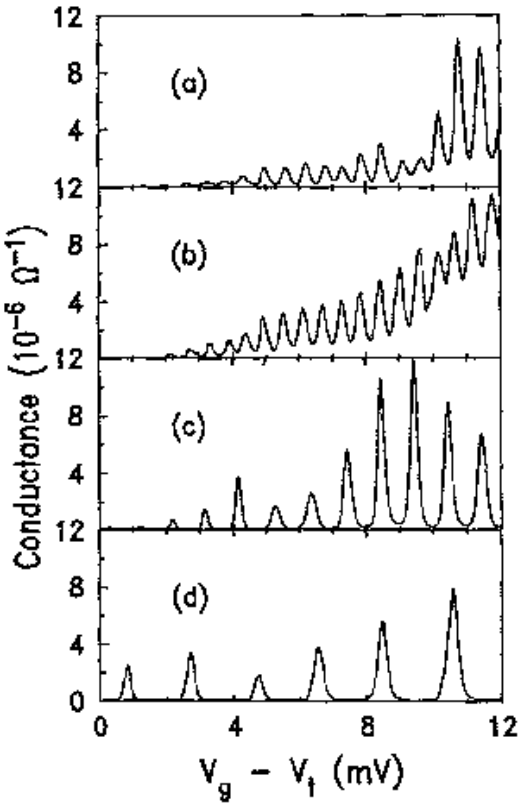

Figure 22: The back gate voltage dependence of the conductance of single electron tunneling transistor devices at low temperature $T = 50$mK. (a) and (b) are for samples with the same barrier separation, (c) and (d) are for progressively lower barrier distance and exhibit correspondingly larger periodicity of the oscillations (from [60]).

The nonlinear transport properties can then be used to investigate the properties of few interacting electrons, confined in a quantum dot. Quantum dots are sometimes called artificial atoms and the transport experiments [66, 70, 71] in the linear and non-linear regime as well as under the influence of electromagnetic radiation [72] allow to study their properties systematically. This permits to study confined correlated many-body quantum systems and represents an important tool for fundamental research in quantum physics [73]. As an example, electronic correlation effects like the Kondo effect can be studied in the transport properties of very small single electron transistor devices [74, 75].

Making structures with two [76], three [77] and more coupled quantum dots, even artificial molecules can be investigated experimentally.

3.3.2 Applications

Since the conductance of a single electron transistor depends strongly on the gate voltage, it can in fact be used as a transistor. But in addition to the usual functionality of a transistor, the conductance of a single electron transistor exhibits oscillations as a function of the gate voltage which might be used in electrical circuits. Since a single electron transistor it is extremely sensitive, it might be used to amplify quantum signals [78], like the ones obtained in the read-out of a future quantum computer.

Since the conductance of a single electron transistor can vary by several orders of magnitude with a small change of the gate voltage, such a setup is also an extremely sensitive electrometer, capable of measuring fractions of an electronic charge [79].

Most important, the Coulomb blockade allows to manipulate single electrons in a controlled way, devices containing tunable tunnel junctions and quantum dots can be used to count electrons or to create well defined currents

$$I = nef \tag{93}$$

when f is the frequency of the applied ac control voltages and n is the number of electrons transferred per cycle [80, 81]. This has important metrological applications and might lead to a current standard in the close future. Metrologically important accuracy has already been achieved when a counted number of electrons was used to charge a capacitor [82], paving the road towards a novel capacitance standard.

Making the quantum dot structure extremely small ($\sim$ 5nm), single electron tunneling can be observed even at room temperature. Without the need of extremely low temperatures as in the first experiments, single electron tunneling becomes interesting for different purposes. However, it remains difficult to fabricate quantum dots of so small size and their contacts to the leads in a controlled way.

4 Summary

In this series of lectures, an introduction of the physics of mesoscopic systems was given. In the mesoscopic regime, many interesting and sometimes unexpected effects appear due to the phase coherence of the electronic wave-functions. Some of these effects are very promising for applications in nano-electronic devices or for quantum standards in metrology. The most prominent example, the integer quantum Hall effect, is already used as a resistance standard.

On the other hand, mesoscopic systems provide the possibility to study basic features of quantum mechanics in a controlled way. They

also allow to study directly features of interacting correlated quantum many-body systems. Examples are the fractional quantum Hall effect and the transport spectroscopy of interacting electrons in quantum dots.

In material science, the main subject of the present school, the tendency to produce and investigate materials containing smaller and smaller structures, and having low-dimensional features, leads towards the mesoscopic regime. Therefore, mesoscopic effects are expected to become more and more important in this field of research.

Acknowledgement

It is a pleasure to thank Rodolfo Jalabert for critically reading the manuscript.

References

[1] Yoseph Imry. *Introduction to Mesoscopic Physics*. Oxford University Press, New York, 1997.

[2] Supryio Datta. *Electronic Transport in Mesoscopic Systems*. Cambridge University Press, Cambridge, 1995.

[3] T. Dittrich, P. Hänggi, G.-L. Ingold, B. Kramer, G. Schön, and W. Zwerger. *Quantum Transport and Dissipation*. Wiley-VCH, Weinheim, 1998.

[4] K. K. Choi, D. C. Tsui, and K. Alavi. Dephasing time and one-dimensional localization of two-dimensional electrons in GaAs/Al_xGa_{1-x}As heterostructures. *Phys. Rev. B*, 36(14):7751–7754, November 1987.

[5] R. A. Webb, S. Washburn, C. P. Umbach, and R. B. Laibowitz. Observation of h/e Aharonov-Bohm oscillations in normal-metal rings. *Phys. Rev. Lett.*, 54(25):2696–2699, June 1985.

[6] K. von Klitzing, G. Dorda, and M. Pepper. New method for high-accuracy determination of the fine–structure constant based on quantized Hall resistance. *Phys. Rev. Lett.*, 45(6):494–497, August 1980.

[7] R. E. Prange and S. M. Girvin. *The Quantum Hall Effect*. Springer-Verlag, New York, 1987.

[8] T. Chakraborty and P. Pietiläinen. *The Quantum Hall Effects*. Solid-State Sciences. Springer, Berlin, second edition, 1995.

[9] D. C. Tsui, H. L. Stormer, and A. C. Gossard. Two–dimensional magnetotransport in the extreme quantum limit. *Phys. Rev. Lett.*, 48(22):1559–1562, May 1982.

[10] R. B. Laughlin. Anomalous quantum Hall effect: An incompressible quantum fluid with fractionally charged excitations. *Phys. Rev. Lett.*, 50(18):1395–1398, May 1983.

[11] L. Saminadayar, D. C. Glattli, Y. Jin, and B. Etienne. Observation of the $e/3$ fractionally charged Laughlin quasiparticle. *Phys. Rev. Lett.*, 79(13):2526–2529, September 1997.

[12] P. A. Lee, A. Douglas Stone, and H. Fukuyama. Universal conductance fluctuations in metals: Effects of finite temperature, interactions, and magnetic field. *Phys. Rev. B*, 35(3):1039–1070, January 1987.

[13] A. B. Fowler, A. Hartstein, and R. A. Webb. Conductance in restricted–dimensionality accumulation layers. *Phys. Rev. Lett.*, 48(3):196–199, January 1982.

[14] D. Mailly, M. Sanquer, J.-L. Pichard, and P. Pari. *Europhys. Lett.*, 8:471, 1989.

[15] B. J. van Wees, H. van Houten, C. W. J. Beenakker, J. G. Williamson, L. P. Kouwenhoven, D. van der Marel, and C. T. Foxon. Quantized conductance of point contacts in a two-dimensional electron gas. *Phys. Rev. Lett.*, 60(9):848–850, February 1988.

[16] D. A. Wharam, T. J. Thornton, R. Newbury, M. Pepper, H. Ahmed, J. E. F. Frost, D. G. Hasko, D. C. Peacock, D. A. Ritchie, and G. A. C. Jones. One-dimensional transport and the quantisation of the ballistic resistance. *J. Phys. C: Solid State Phys.*, 21:L209–L214, 1988.

[17] B. J. van Wees, L. P. Kouwenhoven, E. M. M. Willems, C. J. P. M. Harmans, J. E. Mooij, H. van Houten, C. W. J. Beenakker, J. G. Williamson, and C. T. Foxon. Quantum ballistic and adiabatic electron transport studied with quantum point contacts. *Phys. Rev. B*, 43(15):12431–12453, May 1991.

[18] J. L. Costa-Krämer, N. García, P. García-Mochales, and P. A. Serena. Nanowire formation in macroscopic metallic contacts: quantum mechanical conductance tapping a table top. *Surf. Sci.*, 342:L1144–L1149, 1995.

[19] F. Hund. *Ann. Phys. (Leipzig)*, 32:102, 1938.

[20] M. Büttiker, Y. Imry, and R. Landauer. Josephson behavior in small normal one-dimensional rings. *Phys. Lett.*, 96A:365, 1983.

[21] Ulrich Eckern and Peter Schwab. Normal persistent currents. *Advances in Physics*, 44(5):387, 1995.

[22] N. Byers and C. N. Yang. Theoretical considerations concerning quantized magnetic flux in superconducting cylinders. *Phys. Rev. Lett.*, 7(2):46–49, July 1961.

[23] V. Chandrasekhar, R. A. Webb, M. J. Brady, M. B. Ketchen, W. J. Gallagher, and A. Kleinsasser. Magnetic response of a single, isolated gold loop. *Phys. Rev. Lett.*, 67(25):3578–3581, December 1991.

[24] Albert Schmid. Persistent currents in mesoscopic rings by suppression of charge fluctuations. *Phys. Rev. Lett.*, 66(1):80–83, January 1991.

[25] Felix von Oppen and Eberhard K. Riedel. Average persistent current in a mesoscopic ring. *Phys. Rev. Lett.*, 66(1):84–87, January 1991.

[26] B. L. Altshuler, Y. Gefen, and Y. Imry. Persistent differences between canonical and grand canonical averages in mesoscopic ensembles: Large parametric orbital susceptibilities. *Phys. Rev. Lett.*, 66(1):88–91, January 1991.

[27] L. P. Lévy, G. Dolan, J. Dunsmuir, and H. Bouchiat. Magnetization of mesoscopic copper rings: Evidence for persistent currents. *Phys. Rev. Lett.*, 64(17):2074–2077, April 1990.

[28] B. Sriram Shastry and Bill Sutherland. Twisted boundary conditions and effective mass in Heisenberg-Ising and Hubbard rings. *Phys. Rev. Lett.*, 65(2):243–246, July 1990.

[29] A. Müller-Groeling, H. A. Weidenmüller, and C. H. Lewenkopf. Interacting electrons in mesoscopic rings. *Europhys. Lett.*, 22(3):193–198, April 1993.

[30] A. Müller-Groeling and H. A. Weidenmüller. Persistent currents in one– and two–dimensional mesoscopic rings: Influence of the Coulomb interaction, impurity scattering, and periodic potential. *Phys. Rev. B*, 49(7):4752–4767, February 1994.

[31] D. Mailly, C. Chapelier, and A. Benoit. Experimental observation of persistent currents in a GaAs-AlGaAs single loop. *Phys. Rev. Lett.*, 70(13):2020–2023, March 1993.

[32] T. Martin, G. Montambaux, and J. Trân Thanh Vân, editors. *Correlated Fermions and Transport in Mesoscopic Systems*, Gif–sur–Yvette, 1996. Editions Frontières. Proceedings of the XXXI$^{\text{st}}$ Rencontres de Moriond.

[33] Neil W. Ashcroft and N. David Mermin. *Solid State Physics*. Saunders College, hrw international edition, 1976. ISBN 0-03-049346-3.

[34] Yigal Meir, Ned S. Wingreen, and Patrick A. Lee. Transport through a strongly interacting electron system: Theory of periodic conductance oscillations. *Phys. Rev. Lett.*, 66(23):3048–3051, June 1991.

[35] G. D. Mahan. *Many-Particle Physics*. Plenum, New York, 2nd edition, 1990.

[36] S. Doniach and E. H. Sondheimer. *Green's Functions for Solid State Physicists*. Benjamin, Reading, Massachusetts, 1974.

[37] A. Douglas Stone and Aaron Szafer. What is measured when you measure a resistance? — The Landauer formula revisited. *IBM J. Res. Develop.*, 32(3):384–413, May 1988.

[38] Daniel S. Fisher and Patrick A. Lee. Relation between conductivity and transmission matrix. *Phys. Rev. B*, 23(12):6851–6854, June 1981.

[39] B. Velicky, J. Mašek, and B. Kramer. ac–conductance of an infinite ideal quantum wire in an electric field with arbitrary spatial distribution. *Phys. Lett. A*, 140(7,8):447–450, October 1989.

[40] J. Mašek and B. Kramer. On the conductance of finite systems in the ballistic regime: dependence on Fermi energy, magnetic field, frequency, and disorder. *Z. Phys. B*, 75:37–45, 1989.

[41] R. Landauer. Spatial variation of currents and fields due to localized scatterers in metallic conduction. *IBM J. Res. Develop.*, 1:223–231, June 1957.

[42] Ulrich Weiss. *Quantum Dissipative Systems*, volume 2 of *Series in Modern Condensed Matter Physics*. World Scientific, Singapore, 1993.

[43] R. Landauer. Electrical resistance of disordered one–dimensional lattices. *Phil. Mag.*, 21:863, 1970.

[44] E. N. Economou and C. M. Soukoulis. Static conductance and scaling theory of localization in one dimension. *Phys. Rev. Lett.*, 46(9):618–621, March 1981.

[45] A. Abdellaoui and F. Benamira. Mesoscopic conductance fluctuations in a four probe setup measurement: The Landauer approach. In *Physics of New Materials: Theory and Applications*, 2000. Proceedings of the VII. Petra School of Physics.

[46] Rolf Landauer. Can a length of perfect conductor have a resistance? *Phys. Lett.*, 85A(2):91–93, September 1981.

[47] M. Büttiker. Four–terminal phase–coherent conductance. *Phys. Rev. Lett.*, 57(14):1761–1764, October 1986.

[48] B. Kramer and A. MacKinnon. Localization: theory and experiment. *Rep. Prog. Phys.*, 56:1469–1564, 1993.

[49] R. J. Haug. Edge-state transport and its experimental consequences in high magnetic fields. *Semicond. Sci. Technol.*, 8:131–153, 1993.

[50] D. V. Averin and K. K. Likharev. Single electronics: A correlated transfer of single electrons and cooper pairs in systems of small tunnel junctions. In B. L. Altshuler, P. A. Lee, and R. A. Webb, editors, *Mesoscopic Phenomena in Solids*, chapter 6, pages 173–271. Elsevier Science Publishers B.V., 1991.

[51] M. A. Kastner. The single-electron transistor. *Rev. Mod. Phys.*, 64(3):849–858, July 1992.

[52] P. Delsing, K. K. Likharev, L. S. Kuzmin, and T. Claeson. Effect of high-frequency electrodynamic environment on the single-electron tunneling in ultrasmall junctions. *Phys. Rev. Lett.*, 63(11):1180–1183, September 1989.

[53] D. V. Averin and K. K. Likharev. *J. Low Temp. Phys.*, 1986.

[54] Hermann Grabert. Single charge tunneling: a brief introduction. *Z. Phys. B*, 85:319–325, 1991.

[55] Michel H. Devoret, Daniel Esteve, and Cristian Urbina. Single–electron transfer in metallic nanostructures. *Nature*, 360:547–553, December 1992.

[56] M. H. Devoret, D. Esteve, H. Grabert, G.-L. Ingold, H. Pothier, and C. Urbina. Effect of the electromagnetic environment on the Coulomb blockade in ultrasmall tunnel junctions. *Phys. Rev. Lett.*, 64(15):1824–1827, April 1990.

[57] I. Giaever and H. R. Zeller. *Phys. Rev. Lett.*, 1968.

[58] T. A. Fulton and G. J. Dolan. Observation of single-electron charging effects in small tunnel junctions. *Phys. Rev. Lett.*, 59(1):109–112, July 1987.

[59] C. W. J. Beenakker. Theory of Coulomb–blockade oscillations in the conductance of a quantum dot. *Phys. Rev. B*, 44(4):1646, July 1991.

[60] U. Meirav, M. A. Kastner, and S. J. Wind. Single–electron charging and periodic conductance resonances in GaAs nanostructures. *Phys. Rev. Lett.*, 65(6):771–774, August 1990.

[61] Venkat Chandrasekhar, Zvi Ovadyahu, and Richard A. Webb. Single–electron charging effects in insulating wires. *Phys. Rev. Lett.*, 67(20):2862–2865, November 1991.

[62] Michel Devoret and Christian Glattli. Single–electron transistors. *Physics World*, pages 29–33, September 1998.

[63] Dietmar Weinmann, Wolfgang Häusler, and Bernhard Kramer. Transport properties of quantum dots. *Ann. Physik*, 5:652–695, 1996.

[64] J. Weis, R. J. Haug, K. Klitzing, and K. Ploog. Transport spectroscopy of a confined electron system under a gate tip. *Phys. Rev. B*, 46(19):12837–12840, November 1992.

[65] A. T. Johnson, L. P. Kouwenhoven, W. de Jong, N. C. van der Vaart, and C. J. P. M. Harmans. Zero–dimensional states and single electron charging in quantum dots. *Phys. Rev. Lett.*, 69(10):1592–1595, September 1992.

[66] J. Weis, R. J. Haug, K. v. Klitzing, and K. Ploog. Competing channels in single–electron tunneling through a quantum dot. *Phys. Rev. Lett.*, 71(24):4019–4022, December 1993.

[67] D. Weinmann, W. Häusler, W. Pfaff, B. Kramer, and U. Weiss. Spin blockade in non–linear transport through quantum dots. *Europhys. Lett.*, 26(6):467–472, May 1994.

[68] Dietmar Weinmann, Wolfgang Häusler, and Bernhard Kramer. Spin blockades in linear and nonlinear transport through quantum dots. *Phys. Rev. Lett.*, 74(6):984–987, February 1995.

[69] Kristian Jauregui, Wolfgang Häusler, Dietmar Weinmann, and Bernhard Kramer. Signatures of electron correlations in the transport properties of quantum dots. *Phys. Rev. B*, 53(4):R1713–R1716, January 1996.

[70] S. Tarucha, D. G. Austing, T. Honda, R. J. van der Hage, and L. P. Kouwenhoven. Shell filling and spin effects in a few electron quantum dot. *Phys. Rev. Lett.*, 77(17):3613–3616, October 1996.

[71] S. Tarucha, D. G. Austing, Y. Tokura, W. G. van der Wiel, and L. P. Kouwenhoven. Direct Coulomb and exchange interaction in artificial atoms. *Phys. Rev. Lett.*, 84(11):2485–2488, March 2000.

[72] T. H. Oosterkamp, L. P. Kouwenhoven, A. E. A. Koolen, N. C. van der Vaart, and C. J. P. M. Harmans. Photon sidebands of the ground state and first excited state of a quantum dot. *Phys. Rev. Lett.*, 78(8):1536–1539, February 1997.

[73] Patrick A. Lee. Few electron nanostructures: a laboratory for studying strongly interacting systems. *Physica B*, 189:1–5, 1993.

[74] D. Goldhaber-Gordon, Hadas Shtrikman, D. Mahalu, David Abusch-Magder, U. Meirav, and M. A. Kastner. Kondo effect in a single-electron transistor. *Nature*, 391(6663):156 – 159, 1998.

[75] J. Schmid, J. Weis, K. Eberl, and K. v. Klitzing. Absence of odd-even parity behavior for Kondo resonances in quantum dots. *Phys. Rev. Lett.*, 84(25):5824–5827, June 2000.

[76] R. H. Blick, R. J. Haug, J. Weis, D. Pfannkuche, K. v. Klitzing, and K. Eberl. Single–electron tunneling through a double quantum dot: The artificial molecule. *Phys. Rev. B*, 53(12):7899–7902, March 1996.

[77] F. R. Waugh, M. J. Berry, D. J. Mar, R. M. Westervelt, K. L. Campman, and A. C. Gossard. Single–electron charging in double and triple quantum dots with tunable coupling. *Phys. Rev. Lett.*, 75(4):705–708, July 1995.

[78] Michel H. Devoret and Robert J. Schoelkopf. Amplifying quantum signals with the single-electron transistor. *Nature*, 406(6799):1039–1046, 2000.

[79] R. J. Schoelkopf, P. Wahlgren, A. A. Kozhevnikov, P. Delsing, and D. E. Prober. The radio–frequency single–electron transistor (RF-SET): A fast and ultrasensitive electrometer. *Science*, 280:1238–1242, May 1998.

[80] L. J. Geerligs, V. F. Anderegg, P. A. M. Holweg, J. E. Mooij, H. Pothier, D. Esteve, C. Urbina, and M. H. Devoret. Frequency–locked turnstile device for single electrons. *Phys. Rev. Lett.*, 1990.

[81] L. P. Kouwenhoven, A. T. Johnson, N. C. van der Vaart, C. J. P. M. Harmans, and C. T. Foxon. Quantized current in a quantum-dot turnstile using oscillating tunnel barriers. *Phys. Rev. Lett.*, 67(12):1626–1629, September 1991.

[82] Mark W. Keller, John M. Martinis, Neil M. Zimmerman, and Andrew H. Steinbach. Accuracy of electron counting using a 7-junction electron pump. *Appl. Phys. Lett.*, 69(12):1804–1806, September 1996.